bioRxiv preprint doi: https://doi.org/10.1101/458810; this version posted October 31, 2018. The copyright holder for this preprint (which was not certified by peer review) is the author/funder. All rights reserved. No reuse allowed without permission.

A risk-reward tradeoff of high ribosome production in proliferating cells

Blake W. Tye[1,2], Nicoletta Commins[3], Michael Springer[3], David Pincus[4], L. Stirling Churchman[1*]

Affiliations:
[1]Department of Genetics, Harvard Medical School, Boston, MA 02115
[2]Program in Chemical Biology, Harvard University, Cambridge, MA 02138
[3]Department of Systems Biology, Harvard Medical School, Boston, MA 02115
[4]Whitehead Institute for Biomedical Research, Cambridge, MA 02142
*Correspondence to: churchman@genetics.med.harvard.edu

Abstract:

To achieve maximal growth, cells must manage a massive economy of ribosomal proteins (r-proteins) and RNAs (rRNAs), which are required to produce thousands of new ribosomes every minute. Although ribosomes are essential in all cells, disruptions to ribosome biogenesis lead to heterogeneous phenotypes. Here, we modeled these perturbations in *Saccharomyces cerevisiae* and show that challenges to ribosome biogenesis result immediately in acute loss of proteostasis (protein folding homeostasis). Imbalances in the synthesis of r-proteins and rRNAs lead to the rapid aggregation of newly synthesized orphan r-proteins and compromise essential cellular processes. In response, proteostasis genes are activated by an Hsf1-dependent stress response pathway that is required for recovery from r-protein assembly stress. Importantly, we show that exogenously bolstering the proteostasis network increases cellular fitness in the face of challenges to ribosome assembly, demonstrating the direct contribution of orphan r-proteins to cellular phenotypes. Our results highlight ribosome assembly as a linchpin of cellular homeostasis, representing a key proteostasis vulnerability for rapidly proliferating cells that may be compromised by diverse genetic, environmental, and xenobiotic conditions that generate orphan r-proteins.

bioRxiv preprint doi: https://doi.org/10.1101/458810; this version posted October 31, 2018. The copyright holder for this preprint (which was not certified by peer review) is the author/funder. All rights reserved. No reuse allowed without permission.

Introduction:

Ribosomes are large macromolecular machines that carry out cellular protein synthesis. Cells dedicate up to half of all protein and RNA synthesis to the production of ribosomal protein (r-protein) and RNA (rRNA) components required to assemble thousands of new ribosomes every minute (Warner, 1999). rRNAs and r-proteins are coordinately synthesized and matured in the nucleolus and cytosol, respectively, in response to growth cues (Lempiäinen and Shore, 2009). R-proteins are co- and post-translationally folded, requiring general chaperones as well as dedicated chaperones called escortins (Pillet et al., 2017). Thus, ribosome assembly requires the coordinated synthesis and assembly of macromolecules across cellular compartments, and must be perform at extremely high rates.

The balanced synthesis of rRNA and r-protein components in proliferating cells is frequently disrupted by genetic and extracellular insults, leading to a wide range of phenotypes. Environmental stressors, such as heat shock and viral infection, and xenobiotics, such as DNA-damaging agents used as chemotherapeutics, interfere with rRNA processing and nucleolar morphology (Burger et al., 2010; Kos-Braun et al., 2017; Liu et al., 1996; Pelham, 1984). In zebrafish, and possibly in humans, hemizygous loss of r-protein genes can drive cancer formation (Amsterdam et al., 2004; Goudarzi and Lindström, 2016). Diverse loss-of-function mutations in genes encoding r-proteins, r-protein assembly factors, and rRNA synthesis machinery result in tissue-specific pathologies in humans (ribosomopathies), such as red blood cell differentiation defects in patients with Diamond–Blackfan anemia (DBA) (Draptchinskaia et al., 1999; Khajuria et al., 2018; Narla and Ebert, 2010). Not all of the phenotypes caused by defects in ribosome biogenesis are wholly deleterious: in budding yeast, loss of r-protein genes increases stress resistance and replicative lifespan and reduces cell size and growth (Jorgensen et al., 2004; Steffen et al., 2008, 2012), and mutations in r-protein genes in *C. elegans* also extend lifespan. Collectively, then, despite the fact that ribosomes are required in all cells, disruptions in ribosome biogenesis lead to an array of phenotypic consequences that depend strongly on the cellular context.

Phenotypes resulting from perturbations to ribosome assembly have both translation-dependent and -independent origins. As expected, when ribosomes are less abundant, biomass accumulation slows and growth rates decreases. Furthermore, reduced ribosome concentrations alter global translation efficiencies, impacting the proteome in cell state–specific ways (Khajuria et al., 2018; Mills and Green, 2017). In many cases, however, cellular growth is affected before ribosome pools have appreciably diminished, indicating that perturbations of ribosome assembly have translation-independent or extraribosomal effects. The origins of these effects are not well understood, but may involve unassembled r-proteins. In many ribosomopathies, excess r-proteins directly interact with and activate p53, presumably as a consequence of imbalanced r-protein stoichiometry. However, p53 activation is not sufficient to explain the extraribosomal phenotypes observed in ribosomopathies or in model organisms experiencing disrupted ribosome biogenesis (James et al., 2014).

bioRxiv preprint doi: https://doi.org/10.1101/458810; this version posted October 31, 2018. The copyright holder for this preprint (which was not certified by peer review) is the author/funder. All rights reserved. No reuse allowed without permission.

To determine how cells respond and adapt to perturbations in ribosome assembly, we took advantage of fast-acting chemical-genetic tools in *Saccharomyces cerevisiae* to rapidly and specifically disrupt various stages of ribosome assembly. These approaches capture the kinetics of cellular responses, avoid secondary effects, and are far more specific than available fast-acting chemicals that disrupt ribosome assembly, such as transcription inhibitors, topoisomerase inhibitors, and nucleotide analogs. Furthermore, by performing this analysis in yeast, which lacks p53, we obtained insight into the fundamental, p53-independent consequences of perturbations of ribosome biogenesis.

We found that in the wake of perturbed ribosome assembly, cells experience a rapid collapse of protein folding homeostasis that independently impacts cell growth. This proteotoxicity is due to accumulation of excess newly synthesized r-proteins, which are found in insoluble aggregates. Under these conditions, cells launch an adaptive proteostasis response, consisting of Heat Shock Factor 1 (Hsf1)-dependent upregulation of chaperone and degradation machinery, which is required for adapting to r-protein assembly stress. Bolstering the proteostasis network by exogenously activating the Hsf1 regulon increases cellular fitness when ribosome assembly is perturbed. The high degree of conservation of Hsf1, proteostasis networks, and ribosome assembly indicates that the many conditions that disrupt ribosome assembly and orphan r-proteins in other systems may also drive proteostasis collapse, representing a key extraribosomal vulnerability in cells with high rates of ribosome production.

Results:

Imbalanced rRNA:r-protein synthesis elicits upregulation of proteostasis machinery via Heat Shock Factor 1 (Hsf1)

Ribosome biogenesis commences in the nucleolus, where rRNA is synthesized and processed, and many r-proteins are assembled concomitantly (Figure 1A). As a first class of disruption to ribosome biogenesis, we examined the consequences of imbalances in rRNA and r-protein production. Specifically, we focused on nuclease factors involved in several different stages of processing rRNAs for the large (60S) ribosomal subunit: endonuclease Las1, 5'-exonucleases Rat1 and Rrp17, and 3'-exonuclease Rrp44/Dis3 (exosome) (Kressler et al., 2017; Turowski and Tollervey, 2015; Woolford and Baserga, 2013). We tagged the target molecules with an auxin-inducible degron (AID), which allows rapid depletion of a tagged protein upon addition of the small molecule auxin (Nishimura et al., 2009), thereby acutely shutting down production of mature rRNA (Figure 1B). The rRNA processing factors were depleted by 75–90% within 10–20 min of auxin addition, and precursor rRNA (pre-rRNA) accumulated by 20 min, confirming that depletion of these factors rapidly interfered with rRNA processing (Figures 1C and 1D). Depletion also led to a detectable reduction in the level of free 60S subunits, indicating that the cell was failing to assemble new 60S, but had no effect on the mature ribosome pool (Figure S1A).

To determine whether cells respond directly to disrupted rRNA production, we explored the immediate transcriptional response following depletion of these factors. For this purpose, we auxin-treated (or mock-treated) each strain for 20 min, and then performed

bioRxiv preprint doi: https://doi.org/10.1101/458810; this version posted October 31, 2018. The copyright holder for this preprint (which was not certified by peer review) is the author/funder. All rights reserved. No reuse allowed without permission.

expression profiling by RNA-seq. WT cells exhibited no alteration of the transcriptome in the presence of auxin, whereas each AID-tagged strain exhibited the same compact response. Remarkably, the induced genes are known targets of Heat Shock Factor 1 (Hsf1), a conserved master transcription factor that controls protein folding and degradation capacity in stress, aging, and disease (Akerfelt et al., 2010) (Figure 1E). Hsf1 directly controls ~50 genes encoding proteostasis factors, including protein folding chaperones (*SSA1/4* (Hsp70), *HSP82* (Hsp90), co-chaperones), aggregate clearance factors (*BTN2*, *HSP42*, *HSP104*), the transcription factor that regulates proteasome abundance (*RPN4*), and ubiquitin (*UBI4*) (Solís et al., 2016). Upregulation of Hsf1-dependent genes coincided with an increase in Hsf1 occupancy at their promoters (Figure S1B) and was independent of the translational stalling pathway (Rqc2, Figure S1C). Hsf1-target transcripts, measured by Northern blot, were maintained at high levels over an 80-min time-course of auxin treatment (Figure S1D). AID-tagged Rrp17 acted as a partial loss-of-function allele, as indicated by the accumulation of pre-rRNA even in the absence of auxin and reduced cell growth (Figure 1D and data not shown), potentially explaining the mild and more transient upregulation of Hsf1 target transcripts following auxin addition in the strain expressing this protein. Nevertheless, depletion of all four rRNA processing factors each led to strong and specific activation of the Hsf1 regulon.

Importantly, we ruled out the possibility that the depletion strategy itself resulted in Hsf1 activation. Depletion of several factors not involved in rRNA processing via AID did not activate Hsf1, including the RNA surveillance exonuclease Xrn1, mRNA decapping enzyme Dxo1, and transcription termination factor Rtt103 (Figures S2A,B). Additionally, nuclear depletion of an rRNA processing factor using an orthogonal method that does not require proteasome-mediated degradation (“anchor-away”) (Haruki et al., 2008) likewise led to Hsf1 activation, whereas anchor-away depletion of another nuclear protein did not (Figures S2C–F).

Stress conditions and xenobiotics in yeast characteristically activate a “general” environmental stress response (ESR), driven by the transcription factors Msn2/4, which rewires metabolism and fortify cells against further stress (Gasch et al., 2000). Strikingly, Msn2/4-dependent ESR genes were not activated after depletion of rRNA processing factors (Figure 1E). By contrast, treatment of WT cells with the oxidative agent diamide for 15 min potently activated both Hsf1- and Msn2/4-dependent genes, as expected (Figure 1E). Highly specific activation of Hsf1 in the absence of ESR has only been observed in circumstances in which cellular proteostasis is acutely strained: treatment with azetidine-2-carboxylic acid (AZC), a proline analog that interferes with nascent protein folding, resulting in aggregation (Trotter et al., 2002), or overexpression of an aggregation-prone mutant protein (Geiler-Samerotte et al., 2011). Comparison of the kinetics of pre-rRNA and Hsf1-dependent transcript accumulation revealed that cells activate Hsf1 within minutes after rRNA processing is disrupted, indicating a rapid strain on proteostasis, as observed in instantaneous heat shock (Figure S1E).

The results of acute disruption of rRNA processing suggest that Hsf1 is activated by an excess of newly synthesized r-proteins relative to rRNAs. To determine whether the

bioRxiv preprint doi: https://doi.org/10.1101/458810; this version posted October 31, 2018. The copyright holder for this preprint (which was not certified by peer review) is the author/funder. All rights reserved. No reuse allowed without permission.

reverse phenomenon (i.e., a surplus of rRNAs relative to new r-proteins) could also activate Hsf1, we treated cells with rapamycin to inhibit r-protein expression by inactivating TORC1 (Figure 1F). During the first 15–30 min of low-dose rapamycin treatment, cells strongly repress synthesis of r-proteins while maintaining normal levels of rRNA transcription (Reiter et al., 2011). Precursor rRNA accumulated due to r-protein limitation, as expected, but the Hsf1-dependent gene *BTN2* was not upregulated during rapamycin treatment (Figure 1G). Similarly, halting translation, and thus r-protein synthesis, with cycloheximide (CHX) resulted in pre-rRNA accumulation but no upregulation *of BTN2*. On the basis of these findings, we conclude that when r-proteins are in excess relative to what can be assembled into ribosomes, yielding orphan r-proteins, cells activate a proteostatic stress response driven by Hsf1.

Orphan r-proteins are sufficient to activate the Hsf1 regulon

As an orthogonal means of testing the model that orphan r-proteins activate the Hsf1 regulon, we directly inhibited assembly of r-proteins. To this end, we treated cells with a small molecule, diazaborine (DZA), that blocks cytoplasmic assembly of several r-proteins into the 60S subunit by specifically inhibiting the ATPase Drg1 (Loibl et al., 2014) (Figure 2A). Screens for DZA resistance have yielded only mutations in factors involved in drug efflux and the gene encoding the drug's mechanistic target, *DRG1*, indicating that the compound is highly specific (Wendler et al., 1997). Over a time-course of moderate, sublethal DZA treatment, the Hsf1-dependent transcripts *BTN2* and *HSP82* strongly accumulated by 15 min, whereas the Msn2/4-dependent transcript *HSP12* exhibited no response (Figure 2B). Moreover, Hsf1-dependent transcripts returned to basal levels at 90 min, indicating that Hsf1 activation was an adaptive response. Importantly, a DZA-resistant point mutant of Drg1 (V725E) (Loibl et al., 2014) restored cell growth and reduced accumulation of Hsf1-dependent transcripts, confirming that DZA contributes to Hsf1 activation via the expected mechanism (Figure S3). Consistent with a functional role of Hsf1 activation, we found that DZA treatment protected cells from subsequent lethal heat stress (thermotolerance) (Figure S4). In cells treated with DZA for 15 or 45 min, RNA-seq revealed activation of the same response that was induced by depletion of rRNA processing factors: upregulation of Hsf1-dependent proteostasis genes in the absence of Msn2/4-dependent general stress genes (Figure 2C). Furthermore, by 45 min, cells upregulated proteasome subunits ~2-fold, consistent with the early Hsf1-dependent upregulation of the proteasome-regulatory transcription factor *RPN4* (Figure 2D) (Fleming et al., 2002).

As another means to inhibit r-protein assembly, we depleted dedicated r-protein chaperones, called escortins (Kressler et al., 2012; Pillet et al., 2017). Each escortin binds a specific newly synthesized r-protein and brings it to the assembling ribosome, preventing aberrant aggregation (Figure 2E). We generated AID-tagged strains for the Rps26 escortin Tsr2, whose mutation in human cells leads to DBA (Khajuria et al., 2018). We also analyzed two other escortins, Sqt1 (Rpl10) and Yar1 (Rps3), and performed a time-course of auxin treatment for all three. Each escortin was depleted ~70% by 20 min. Northern blots revealed accumulation of *BTN2* and *HSP82* mRNAs by 10–20 min, with no change in the level of

bioRxiv preprint doi: https://doi.org/10.1101/458810; this version posted October 31, 2018. The copyright holder for this preprint (which was not certified by peer review) is the author/funder. All rights reserved. No reuse allowed without permission.

Msn2/4-regulated *HSP12* mRNA (Figure 2F). Both Rps26 and Rps3 are assembled into the pre-40S in the nucleus, whereas Rpl10 is the last r-protein assembled into the ribosome and facilitates subunit joining. Thus, either by inhibition of Drg1 or depletion of escortins, orphan r-proteins are sufficient to activate the Hsf1 regulon. Accordingly, we refer to the stress imparted by orphan r-proteins as ribosomal protein assembly stress (RPAS).

Compromised r-protein gene expression and translational output during RPAS

In addition to the upregulation of the Hsf1 regulon in RPAS, we also observed down-regulation of some genes. Intriguingly, the set of downregulated genes comprised mostly r-protein genes (Figures 3A,B). Under many stress conditions, both r-protein genes and assembly factor genes, collectively termed the ribosome biogenesis (RiBi) regulon, are repressed through Tor-dependent signaling (Jorgensen et al., 2004; Marion et al., 2004; Urban et al., 2007) (e.g., oxidative stress by diamide, Figures 3A,B). Therefore, we suspected that the specific down-regulation of r-protein genes, but not assembly factors, in RPAS would not be executed through Tor. Indeed, cells treated with DZA for 15 or 45 min exhibited no change in the level of the TORC1 activity reporter phos-Rps6 (González et al., 2015) (Figure 3F).

Many stress conditions lead to global translational repression, mediated in part by the kinase Gcn2, and enable specialized or cap-independent translation programs that aid in coping with the stress (Wek, 2018). Previous experiments with DZA showed that translation is downregulated shortly after treatment (Pertschy et al., 2004). To determine whether translation is repressed in RPAS, we monitored the synthesis of various V5-tagged ORFs. Transcription of V5-tagged transgenes was activated by the synthetic transcription factor Gal4–estradiol receptor (ER)–Msn2 activation domain (AD) (GEM) upon the addition of estradiol (Stewart-Ornstein et al., 2012) (Figure 3C). Under normal conditions, we found that the V5-tagged proteins began to accumulate after 10 minutes (Figure 3D). To determine the effect of RPAS on translational output, we briefly treated ORF-V5 strains with estradiol followed by DZA for 20 minutes and assessed the level of protein accumulation. All ORFs, including GFP-V5, accumulated to lower levels when cells were treated with DZA, consistent with a rapid reduction in translational output under RPAS (Figure 3E). Because DZA could achieve a maximal reduction of 20% in the ribosome pool in a 20-minute experiment, this >50% reduction in synthesis cannot be explained by a diminishing ribosome pool. Interestingly, the reduction in translational capacity is not mediated through Gcn2, as its reporter phos-eIF2α did not accumulate during DZA treatment (Dever et al., 1992) (Figure 3F). In sum, we observed compromised r-protein gene transcription and global translational output during RPAS independent of canonical signaling pathways.

Aggregation of orphan r-proteins during RPAS

Hsf1 responds to an increased prevalence of misfolded or aggregated proteins, and activates a transcriptional program to resolve these issues. Accordingly, we hypothesized that newly synthesized orphan r-proteins, which are highly aggregation-prone (Jäkel et al., 2002; Koplin et al., 2010), would aggregate after disruptions to ribosome biogenesis.

bioRxiv preprint doi: https://doi.org/10.1101/458810; this version posted October 31, 2018. The copyright holder for this preprint (which was not certified by peer review) is the author/funder. All rights reserved. No reuse allowed without permission.

Consistent with this idea, we found that Hsf1 activation by DZA required ongoing translation: pre-treatment with CHX prevented upregulation of Hsf1 targets, supporting the model of proteotoxic orphan r-proteins (Figure 4A). Similarly, Hsf1 activation by depletion of the rRNA processing factor Rat1 was fully inhibited by CHX pre-treatment (Figure S5A).

To test for the presence of protein aggregation in DZA-treated cells, we used a sedimentation assay that separates soluble proteins from large, insoluble assemblies (Figure 4B) (Wallace et al., 2015). As a positive control, we induced global protein misfolding by AZC and observed gross protein aggregates associated with disaggregases Hsp70 and Hsp104 (Figure 4C). By contrast, RPAS induced by DZA treatment resulted in no such gross protein aggregation, even at 40 minutes.

We next asked whether newly synthesized r-proteins aggregated during RPAS. Using the estradiol induction system for V5-tagged ORFs, we followed the fate of newly synthesized r-proteins in mock- or DZA-treated cells. We found that newly synthesized Rps26, Rpl10, and Rpl3 shifted dramatically (3–5-fold) to the insoluble fraction upon DZA treatment (Figures 4D,F). Interestingly, the levels of Rpl4 and Rps3 in the pellet increased modestly if at all, possibly due to their distinct biochemical characteristics, protection from aggregation by chaperones, or rapid assembly into precursor ribosome subunits. Treating extracts with the nuclease benzonase did not solubilize aggregated r-proteins, indicating that they were not in RNA- or DNA-dependent assemblies (Figure S5B). To compare these results with the behavior of mature, assembled r-proteins, we grew V5-tagged Rpl10 and Rpl3 strains continuously for 5 hours in estradiol prior to DZA treatment. Under these conditions, most of the tagged r-proteins should reside in mature ribosomes, with a small fraction existing unassembled. After DZA treatment, only a modest amount of tagged r-proteins were present in the pellet, likely due to the small unassembled fraction (Figures 4E,F). We conclude that RPAS results in specific aggregation of orphan r-proteins.

RPAS disrupts nuclear and cytosolic proteostasis

Misfolded and aggregated proteins in the cell are often toxic and have the potential to sequester proteins with essential cellular activities (Gsponer and Babu, 2012; Holmes et al., 2014; and Dobson, 2003). Accordingly, in addition to upregulating proteostasis factors, cells utilize spatial quality control mechanisms to minimize the deleterious effects of aggregates. For example, cells triage proteins into cytosolic aggregate depots, referred to as Q-bodies or CytoQ, where the Hsp40/70 chaperones and Hsp104 disaggregase collaborate to resolve and refold misfolded proteins (Hill et al., 2017; Kaganovich et al., 2008). Aggregates also form in the nucleus, in the intranuclear quality control compartment (INQ), which is thought to be involved in their degradation (Hill et al., 2017; Miller et al., 2015a, 2015b).

We used confocal fluorescence microscopy to follow the localization of the Hsp70 co-chaperone Sis1, which recognizes substrates and participates in nuclear aggregation and degradation (Park et al., 2013; Summers et al., 2013). In normal growing populations, Sis1-YFP was distributed evenly throughout the nucleus except in the nucleoli; the nucleolar protein Cfi1-mKate, which localized at the periphery of the nucleus, exhibited little or no colocalization with Sis1. Upon treatment with DZA, Sis1 drastically relocalized within the

bioRxiv preprint doi: https://doi.org/10.1101/458810; this version posted October 31, 2018. The copyright holder for this preprint (which was not certified by peer review) is the author/funder. All rights reserved. No reuse allowed without permission.

nucleus, moving to the nuclear periphery, where it formed a ring-like structure (Figures 5A–C). At the same time, Cfi1 relocalized from the periphery towards the middle of the nucleus, adjacent to the Sis1 ring structure. The effect of DZA on Sis1 and Cfi1 was completely blocked by inhibiting translation with CHX, consistent with the idea that newly synthesized orphan r-proteins drove the response. The subnuclear relocalization of Sis1 in response to RPAS is consistent with a role in the INQ.

In addition, we analyzed the localization of the disaggregase Hsp104, which recognizes and resolves aggregated proteins (Glover and Lindquist, 1998; Tkach and Glover, 2004). Untreated cells contained one or two Hsp104 foci. Treatment with DZA increased the number of Hsp104 foci, to seven or eight per cell, likely reflecting CytoQ body formation in response to orphan r-proteins (Figure 5D). Based on these data, we conclude that the orphan r-proteins produced as a result of DZA treatment aggregate both in the cytosol, where they are synthesized, and in the nucleus, where most of them are imported and assembled.

Hsf1 and Rpn4 support cell fitness under RPAS

To determine the physiological relevance of Hsf1 activation in response to RPAS, we tested the fitness of *hsf1* mutants and deletions of single Hsf1-dependent genes in DZA. Because *HSF1* is an essential gene, we studied a hyperphosphorylated mutant of Hsf1, *hsf1 po4**, in which all serines are replaced with phospho-mimetic aspartates; this strain grows normally in basal conditions but is a hypoinducer of Hsf1 target genes under heat shock and has a tight temperature-sensitive growth defect (Zheng et al., 2016). We found that *hsf1 po4** cells grew at wild-type rates at 30°C but were very sick under proteotoxic conditions (AZC or 37°C), demonstrating that the *hsf1 po4** allele lacks the ability to cope with proteotoxic stress (Figure 6A). *hsf1 po4** were nearly incapable of growth in DZA (Figure 6B), highlighting the critical role of wild-type Hsf1 in the adaptation to RPAS.

To identify which Hsf1 targets are critical for RPAS adaptation, we investigated the fitness consequence of loss of single Hsf1-dependent genes. In this analysis, we focused on genes whose loss in basal conditions is minimally perturbing but are likely to have important functions in coping with proteotoxic stress. In particular, we deleted factors involved in aggregate formation and dissolution (*HSP104*, *BTN2*, *HSP42*, *HSP26*) and proteasome-mediated degradation (*RPN4*, *TMC1*, *PRE9*); in addition, we deleted the Hsf1-independent gene *HSP12* as a negative control. Because many of these single-gene deletions do not have gross phenotypes, we used a competitive fitness assay to sensitively detect small differences in cell fitness (Breslow et al., 2008; Wang et al., 2015). Individual deletion strains expressing mCherry (mCh) were co-cultured with a wild-type reference strain expressing YFP without treatment (YPD), at 37°C, in 5 mM AZC, DMSO (vehicle), or in 15 or 30 µg/ml DZA. Competitions were maintained over the course of 5 days, and the relative proportion of wild-type and mutant cells was monitored by flow cytometry (Figure 6C). Deletion of most factors had no effect on fitness under any condition tested, likely due to redundancy in the mechanisms responsible for restoring proteostasis (Figure S6). However, loss of the transcription factor *RPN4*, which controls the basal and stress-induced levels of the proteasome (Fleming et al., 2002; Wang et al., 2008), conferred a substantial growth defect

bioRxiv preprint doi: https://doi.org/10.1101/458810; this version posted October 31, 2018. The copyright holder for this preprint (which was not certified by peer review) is the author/funder. All rights reserved. No reuse allowed without permission.

in the presence of DZA (~25-fold more severe than in the absence of drug on day 3), at 37°C, and in the presence of AZC (Figure 6D), suggesting that the proteasome plays a critical role in the response to RPAS. We also found that loss of the only non-essential proteasome subunit, *PRE9*, made cells DZA-resistant (Figure S6). Resistance to some proteotoxic stressors has been observed in weak proteasome mutants, such as *pre9*, and may be the result of compensation by alternate proteasome subunits or elevated basal levels of other proteostasis factors in this mutant (Acosta-Alvear et al., 2015; Brandman et al., 2012; Kusmierczyk et al., 2008; Tsvetkov et al., 2015). As with DZA, *rpn4* and *pre9* cells are sensitive and resistant, respectively, to endoplasmic reticulum (ER) folding stress, which involves clearance of misfolded ER proteins by the proteasome (Kapitzky et al., 2010; Wang et al., 2010). In sum, these data demonstrate that Hsf1 and its target Rpn4, which controls proteasome abundance, support cellular fitness under RPAS.

Proteostatic strain contributes to the growth defect of cells under RPAS

We hypothesized that the proteotoxic stress created by orphan r-proteins contributes to the growth defect of cells under RPAS beyond what would be expected from the effects of a reduced ribosome pool. Because Hsf1 responds to and is required for growth under RPAS, we uncoupled Hsf1 from the proteostasis network and placed it under exogenous control to test whether enhanced proteostasis would modulate the DZA-induced growth defect. For this purpose, we placed a chimeric fusion of the Hsf1 DNA-binding domain with the transactivation domain VP16 ($Hsf1^{DBD}$-VP16) under the control of an estradiol-responsive promoter in a strain lacking wild-type *HSF1*, allowing exogenous upregulation of the Hsf1 regulon by addition of estradiol. The $Hsf1^{DBD}$-VP16 strain was more sensitive to DZA than the wild-type strain, further supporting the importance of wild-type *HSF1* in the RPAS response (Figures 7A,B). To determine whether upregulation of the Hsf1 regulon alleviates the DZA growth defect, we pre-conditioned cells with a 3-hour estradiol treatment, and then measured cell growth after 21 hours of exposure to DZA, AZC, or DMSO (vehicle). Pretreatment with estradiol yielded a >40% growth enhancement in DZA that was independent of changes to cell size. Similar effects were observed after growth in AZC, which induces global proteotoxicity, whereas only a 9% growth rate increase was observed for vehicle-treated cells (Figures 7A,B and S7). These data suggest that the proteotoxic stress of RPAS slows growth, which can be rescued by exogenous amplification of the proteostasis network.

Discussion:

Here, we report an extraribosomal consequence of disrupting ribosome assembly. Our results demonstrate that defects in ribosome biogenesis lead to proteotoxic stress due to accumulation of excess newly synthesized r-proteins, directly impacting cellular fitness (Figure 7C). Orphan r-proteins rapidly aggregate, acutely straining proteostasis and compromising other cellular processes. In turn, the master proteostasis transcription factor Hsf1 is activated to increase the abundance of folding and degradation machineries, likely following sequestration of chaperones such as Hsp40 and Hsp70 by r-protein aggregates (Zheng et al., 2016). The proteostatic response supports cell fitness and is capable of

bioRxiv preprint doi: https://doi.org/10.1101/458810; this version posted October 31, 2018. The copyright holder for this preprint (which was not certified by peer review) is the author/funder. All rights reserved. No reuse allowed without permission.

protecting cells from r-protein assembly stress. Thus, proliferating cells accept a tradeoff between the risk of proteotoxicity and the growth benefits of high ribosome production. The resulting balancing act is vulnerable to disruption by a variety of genetic and chemical insults, necessitating protective mechanisms capable of restoring the balance.

In this study, we focused on rapidly proliferating yeast cells, which dedicate up to half of their biomass accumulation to synthesis of ribosomes. Given the conservation of proteostasis mechanisms and ribosome biogenesis, we suspect that disrupted ribosome assembly might also cause proteotoxic stress in other eukaryotes. Certainly, many conditions have the potential to orphan r-proteins, thereby straining proteostasis. For example, DNA-damaging chemotherapeutic agents like etoposide, camptothecin, and 5-fluorouracil and transcription inhibitors like actinomycin D disrupt the nucleolus and rRNA processing (Burger et al., 2010). Environmental stressors such as heat shock also deform the nucleolus, and many other stressors in yeast cause accumulation of pre-rRNA (Boulon et al., 2010; Kos-Braun et al., 2017). Imbalanced production of r-proteins arises in mutations found in ribosomopathies, as well as in aging (David et al., 2010) and cancer (Guimaraes and Zavolan, 2016). Because ribosome biogenesis is not a constitutive process, but instead fluctuates in response to nutrient availability, stress, cell growth, and differentiation cues (Lempiäinen and Shore, 2009; Mayer and Grummt, 2006), these conditions are likely to acutely challenge ribosome biogenesis and lead to periodic disruptions to proteostasis.

Proteotoxic stress has been extensively linked to overall disruption of cellular homeostasis (Gsponer and Babu, 2012; Holmes et al., 2014; Stefani and Dobson, 2003). Broad proteotoxic stressors like heat and oxidative stress, as well as more specific challenges to protein folding such as growth with aberrant amino acid analogs (e.g., AZC), disrupts cell cycle progression, growth rate, and (at higher levels) viability. Single aggregation-prone proteins are sufficient to reduce cell fitness in a dose-dependent fashion or to cause acute cytotoxicity, as in the case of mutant repeat expanded proteins found in ALS and Huntington's disease (Geiler-Samerotte et al., 2011; Bucciantini et al., 2002). While the molecular basis for how protein aggregates compromise cell health is not fully understood, one demonstrated possibility is that aggregates sequester other proteins with essential functions (Olzscha et al., 2011). Thus, the proteotoxic stress elicited by RPAS has the potential to severely disrupt cellular homeostasis, consistent with our findings that alleviating proteotoxic stress enhances cell growth under RPAS (Figure 7A). Differences among cell types in the ability to withstand proteotoxic conditions might contribute to the phenotypic variability in response to ribosome assembly defects, including the tissue-specific impact of ribosomopathies.

The gene expression response mounted by cells experiencing RPAS provides clues regarding how the cell deals with toxic orphan r-proteins. The requirement for an Hsf1-mediated response suggests that upregulation of the folding and/or degradation machinery contributes to this resolution. The extreme sensitivity of *rpn4* cells to RPAS suggests an important role for proteasome-mediated degradation of orphan r-proteins. Consistent with this, yeast and human cells degrade r-proteins produced in excess, and cells lacking this quality control mechanism contain aggregated r-proteins (McShane et al., 2016; Sung et al.,

bioRxiv preprint doi: https://doi.org/10.1101/458810; this version posted October 31, 2018. The copyright holder for this preprint (which was not certified by peer review) is the author/funder. All rights reserved. No reuse allowed without permission.

2016a, 2016b). Indeed, the proteotoxicity of excess r-proteins may explain why cells evolved mechanisms to prevent their accumulation above stoichiometric levels, even in aneuploid cells (Dephoure et al., 2014).

Activation of the Hsf1 regulon in RPAS is the consequence of newly synthesized r-proteins that cannot reach their normal destination and therefore fail to assemble into a cognate complex, leading to their aggregation. Similarly, the mitochondrial unfolded protein response is activated when assembly of mitochondrial complexes is disrupted (Yoneda et al., 2004). Blocking import of organellar proteins into the ER or mitochondria results in cytosolic proteotoxic stress (Brandman et al., 2012; Wang et al., 2014; Weidberg and Amon, 2018; Wrobel et al., 2015). Thus, aberrant accumulation of orphan proteins – that is, those that do not arrive at their appropriate complex or subcellular location – is a hallmark of proteostasis loss, which is resolved by pathways tailored for each cellular compartment. Consistent with this, under stress such as heat shock, newly synthesized proteins in the cytosol are predominantly targeted for degradation and seed microscopically visible protein aggregates (Medicherla and Goldberg, 2008; Wallace et al., 2015; Zhou et al., 2014), further evidence of their instability relative to mature proteins. In addition, new r-proteins undergo ubiquitination, localize in protein aggregates, and associate with chaperones under heat shock (Fang et al., 2014; Ruan et al., 2017; Shalgi et al., 2013). Given that the nucleolus is morphologically disrupted and recruits chaperones such as Hsp70 under stress, including heat shock and proteasome inhibition (Lam et al., 2007; Liu et al., 1996; Pelham, 1984), it is tempting to speculate that RPAS is responsible, at least in part, for Hsf1 activation in response to various stress stimuli. From this standpoint, r-proteins, due to their exceptionally high abundance, complex assembly pathway, and aggregation-prone nature, simply represent a particularly vulnerable group of proteins.

Particular cell types and cell states, such as tumor cells or differentiating erythropoietic precursors, have exceptional demand for high ribosome production (Mills and Green, 2017; Pelletier et al., 2018). Intriguingly, both of these cell states are unusually sensitive to disruption of proteostasis. Erythroid differentiation is highly reliant on Hsp70 availability, as evidenced by the fact that Hsp70 sequestration can result in the anemic phenotype of beta-thalassemia (Arlet et al., 2014). Similarly, cancer cells are sensitized to small molecules that dampen the proteostasis network (Balch et al., 2008; Joshi et al., 2018). In this work, we showed that exogenous activation of the Hsf1 regulon protects yeast from RPAS. Future studies should seek to determine whether an analogous strategy can therapeutically mitigate phenotypes of disrupted ribosome biogenesis in disease processes.

bioRxiv preprint doi: https://doi.org/10.1101/458810; this version posted October 31, 2018. The copyright holder for this preprint (which was not certified by peer review) is the author/funder. All rights reserved. No reuse allowed without permission.

Acknowledgments:
We thank members of the Churchman lab, F. Winston, R. Kingston, and M. Sonnett for helpful discussions; S. Doris and E. McShane, C. Patil for critical reading of the manuscript; and T. Powers, F. Holstege, V. Denic, and D. Gross for reagents. Microscopy was performed at the Nikon Imaging Center at Harvard Medical School and the W.M. Keck Microscopy Facility at the Whitehead Institute. RNA-seq library preparation and sequencing was performed at the Whitehead Institute and Biopolymers Facility at Harvard Medical School, respectively. This work was supported by the NIH (R01-HG007173 and R01-GM117333 to L.S.C.).

Declaration of Interests:
The authors declare no competing interests.

Data Availability:
All sequencing data has been deposited on Gene Expression Omnibus under accession number GSE114077.

bioRxiv preprint doi: https://doi.org/10.1101/458810; this version posted October 31, 2018. The copyright holder for this preprint (which was not certified by peer review) is the author/funder. All rights reserved. No reuse allowed without permission.

Figure 1

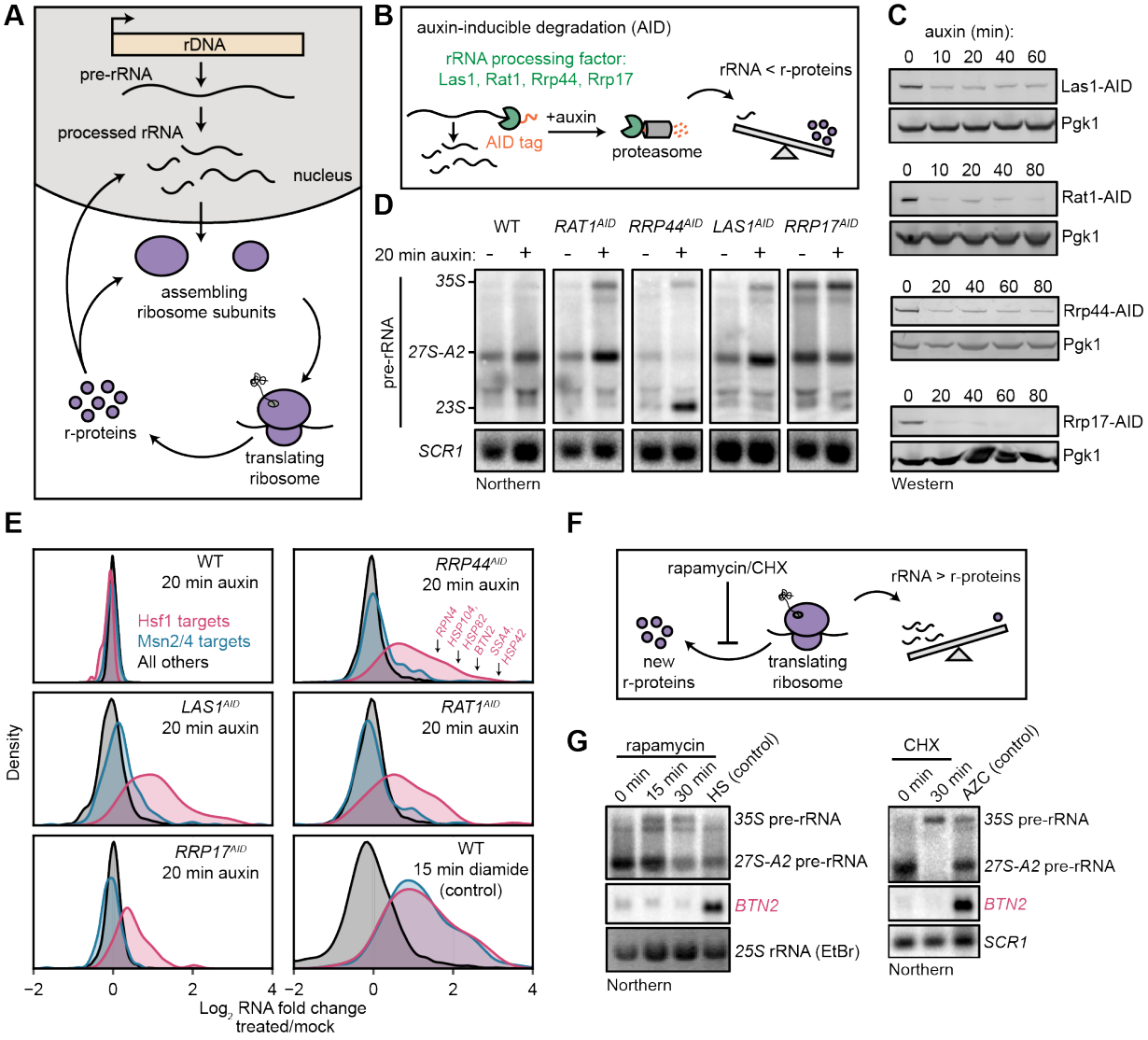

Figure 1. Imbalanced rRNA:r-protein synthesis elicits upregulation of proteostasis machinery via Heat Shock Factor 1 (Hsf1). (**A**) Brief schematic overview of ribosome biogenesis. (**B**) Auxin-inducible degradation (AID) of rRNA processing factors. The C-terminus of the protein is genetically tagged with the AID tag in cells co-expressing the E3 ligase adapter *Os*TIR1. Addition of auxin allows recognition and degradation of AID-tagged proteins by the proteasome. (**C**) Rapid depletion of AID-tagged rRNA processing factors following addition of auxin (100 μM) detected by anti-V5 immunoblot. (**D**) Pre-rRNA accumulation by 20 min of rRNA processing factor depletion. RNA from mock and auxin (20 min) treated cells was analyzed by Northern blot with a probe (017, see Table S3) that recognizes full-length pre-rRNA (35S) and processing intermediates (27S-A2 and 23S) (El Hage et al., 2008). (**E**) Specific upregulation of Hsf1 targets in rRNA processing factor-depleted cells. RNA-seq density plots of $\log_2$ fold change after 20 min auxin treatment (versus mock-treated control), determined from two biological replicates. Hsf1 targets, n=42; Msn2/4 targets, n=207; all others, n=4,912. The oxidative agent diamide (15 min, 1.5 mM) was used as a comparative control. The WT strain treated with auxin also expressed OsTIR1 but lacked any AID-tagged factor. (**F**) Schematic illustrating that rapamycin and CHX treatment acutely shutdown r-protein synthesis ahead of rRNA synthesis leading to an imbalance in ribosome components. (**G**) Northern blots of pre-rRNA and Hsf1-dependent *BTN2* from WT cells treated with rapamycin (200 ng/ml) or CHX (200 μg/ml) for the indicated times. Heat shock (HS, 37°C, 15 min) and azetidine-2-carboxylic acid (AZC, 10 mM, 30 min) were used as positive controls for Hsf1 activation.

bioRxiv preprint doi: https://doi.org/10.1101/458810; this version posted October 31, 2018. The copyright holder for this preprint (which was not certified by peer review) is the author/funder. All rights reserved. No reuse allowed without permission.

Figure 2

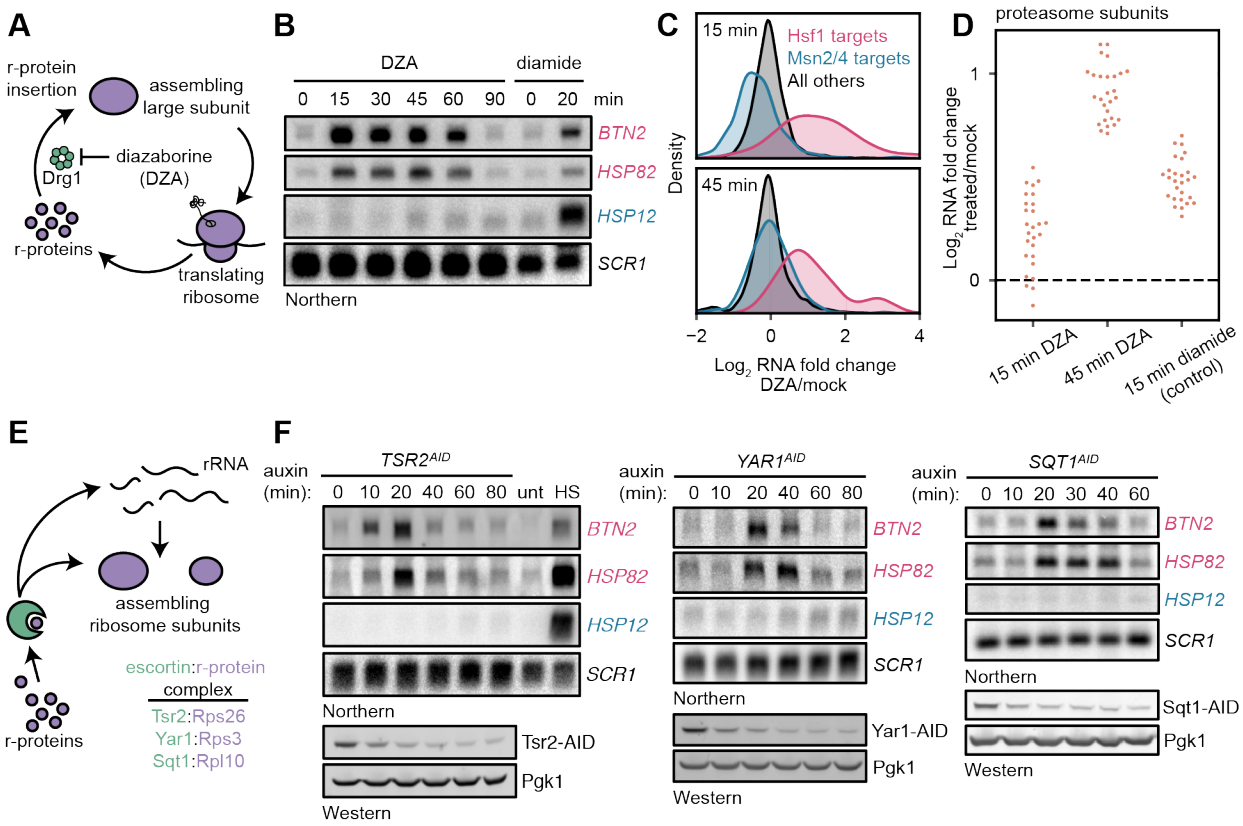

Figure 2. Orphan r-proteins are sufficient to activate the Hsf1 regulon. (**A**) Schematic describing that diazaborine (DZA) inhibits Drg1, preventing r-protein assembly into pre-60S subunits. (**B**) Kinetics of Hsf1 activation following DZA treatment. Northern blot of Hsf1-dependent *BTN2* and *HSP82* and Msn2/4-dependent *HSP12* transcripts from cells treated with DZA (15 μg/ml) for the indicated time. Diamide (1.5 mM) was used as a positive control for Hsf1 and Msn2/4 activation. (**C**) RNA-seq density plots of $\log_2$ fold change after 15 or 45 min DZA treatment (versus DMSO-treated control), determined from two biological replicates. (**D**) Upregulation of proteasome subunits during RPAS. Swarm plot of $\log_2$ fold change after 15 or 45 min DZA or 15 min diamide treatment for transcripts encoding proteasome subunits (n=27). (**E**) Schematic describing how escortins Tsr2, Yar1, and Sqt1 chaperone newly synthesized Rps26, Rps3, and Rpl10, respectively, to assembling ribosomes. (**F**) Western blots showing depletion of AID-tagged Tsr2, Yar1, and Sqt1 and Northern blots for Hsf1-dependent *BTN2* and *HSP82* and Msn2/4-dependent *HSP12* transcripts at the indicated time after auxin addition. Unt, untreated; HS, heat shock.

bioRxiv preprint doi: https://doi.org/10.1101/458810; this version posted October 31, 2018. The copyright holder for this preprint (which was not certified by peer review) is the author/funder. All rights reserved. No reuse allowed without permission.

Figure 3

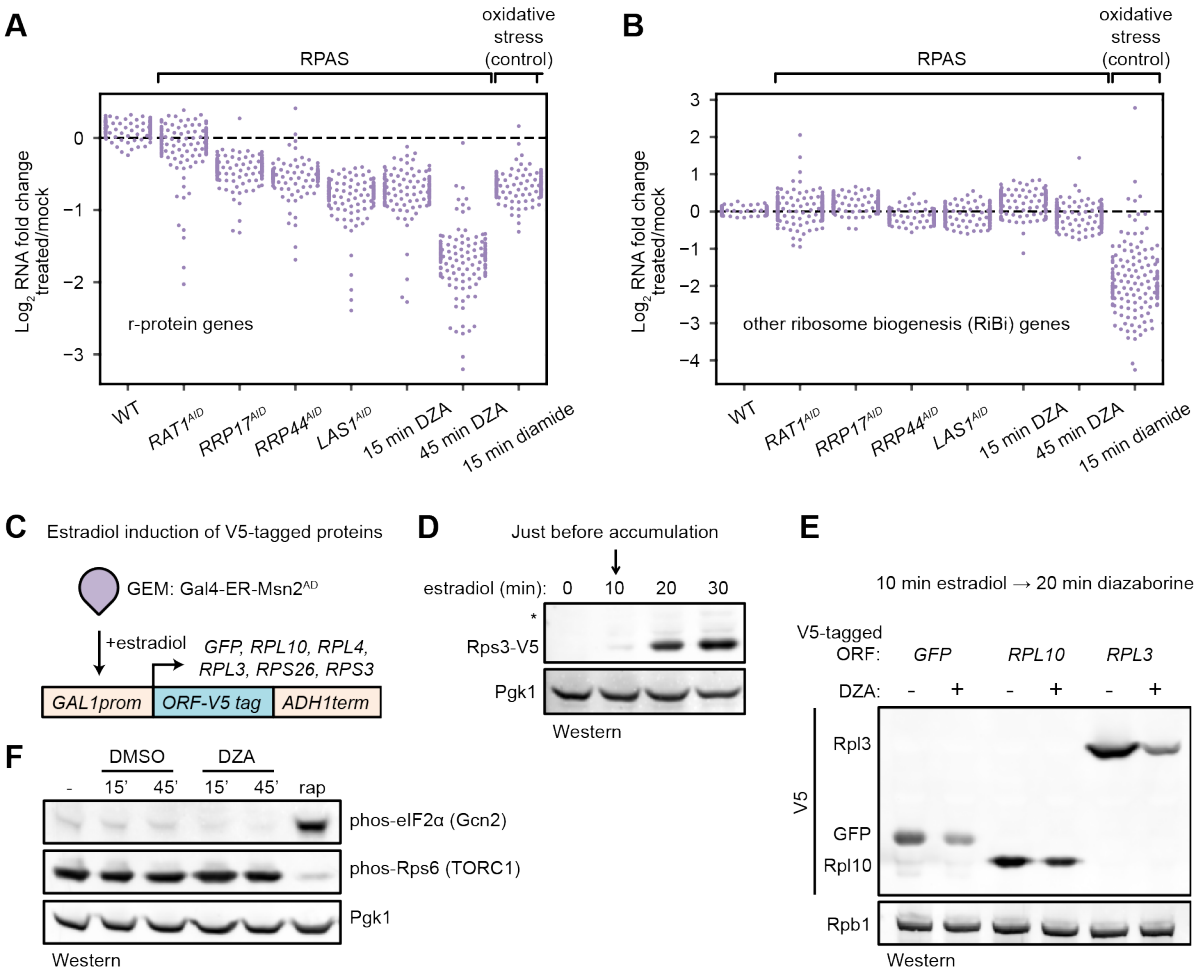

Figure 3. Compromised r-protein gene expression and translational output during RPAS. (**A**) Swarm plot of $\log_2$ fold change of r-protein encoding transcripts in the condition indicated on the x-axis (n=136). (**B**) Swarm plot of $\log_2$ fold change of transcripts encoding ribosome biogenesis (RiBi) factors, excluding r-protein genes, in the condition indicated on the x-axis (n=169). (**C**) Schematic of transgene system for estradiol-inducible expression of V5-tagged ORFs. (**D**) Western blot showing time-course of induction of Rps3-V5 after the indicated time of beta-estradiol (100 nM) addition. (**E**) Strains containing the indicated V5-tagged transgene were induced for 10 min with estradiol and then treated with vehicle (-) or 15 µg/ml DZA (+) for 20 min and analyzed by western blot. (**F**) WT cells were treated with vehicle (DMSO) or DZA for 15 or 45 min and analyzed by western blot. Rapamycin (rap, 200 ng/ml, 45 min) was used as a positive control for altering Gcn2 and TORC1 activity (Dever et al., 1992; González et al., 2015).

bioRxiv preprint doi: https://doi.org/10.1101/458810; this version posted October 31, 2018. The copyright holder for this preprint (which was not certified by peer review) is the author/funder. All rights reserved. No reuse allowed without permission.

Figure 4

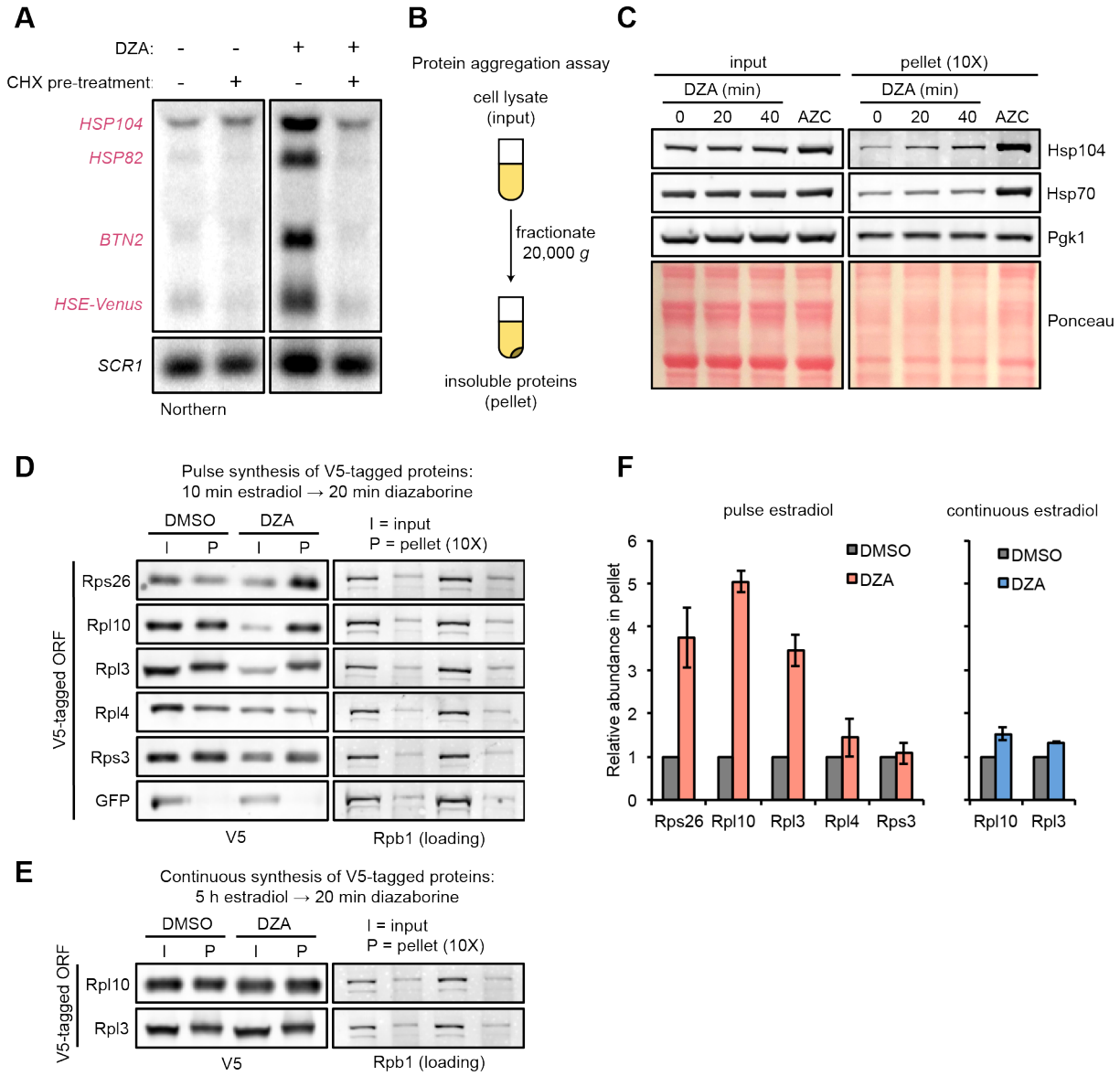

Figure 4. Aggregation of orphan r-proteins during RPAS. (**A**) Cells were mock or CHX (200 µg/ml) treated for 3 min prior to addition of DZA for 20 min and Hsf1 target were detected by Northern blot. *HSE-Venus*, *Venus* transgene downstream of four Hsf1 binding sites (Heat Shock Element, HSE). (**B**) Schematic of the protein aggregation assay. Proteins extracted from cryogenically lysed cells were fractionated by centrifugation at 20,000 *g* for 20 min to pellet insoluble proteins. (**C**) Cells were treated with DZA for 0, 20, or 40 min.Input and insoluble proteins (pellet) were resolved by SDS-PAGE. AZC (10 mM) was used as a control to compare DZA results to a general increase in aggregates in the pellet, by Ponceau staining, and Hsp70 and Hsp104 sedimentation. 10x more of the pellet sample than input sample was loaded to increase sensitivity. (**D**) Strains expressing the indicated V5-tagged r-protein (or GFP as a control) were induced for 10 min with estradiol followed by vehicle (DMSO) or DZA treatment for 20 min. Input and pellet samples for all were analyzed by Western blot. 10x more of the pellet sample than input sample was loaded to increase sensitivity. (**E**) Same as (D), except cells were continuously induced for 5 h with estradiol to label the mature protein pool prior to DMSO or DZA treatment. (**F**) Quantification of the indicated V5-tagged proteins in the pellet fraction versus the input (from panels D and E), normalized to the pellet to input ratio of Rpb1. The ratio was set to 1 for DMSO treated cells. Bar height indicates the average and error bars the range of n=2 biological replicates.

bioRxiv preprint doi: https://doi.org/10.1101/458810; this version posted October 31, 2018. The copyright holder for this preprint (which was not certified by peer review) is the author/funder. All rights reserved. No reuse allowed without permission.

Figure 5

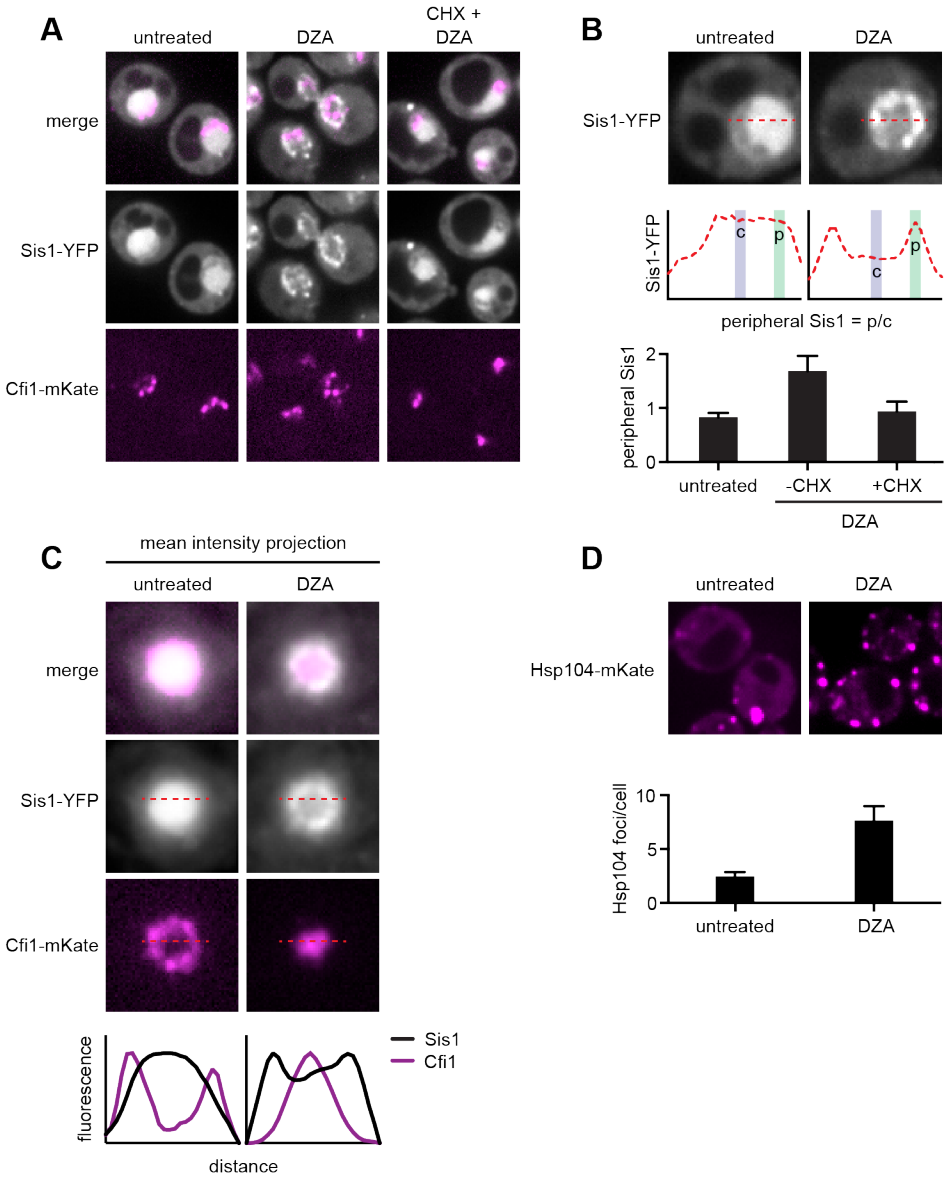

Figure 5. RPAS disrupts nuclear and cytosolic proteostasis. (**A**) Fluorescence micrographs of cells expressing Sis1-YFP and the nucleolar marker Cfi1-mKate after treatment with DZA (5 µg/ml, 30 min) with or without pre-treatment with CHX (200 µg/ml, 5 min). (**B**) Quantification of Sis1 relocalization to the nuclear periphery was done via fluorescence line scans and computed as the ratio of Sis1 signal at the periphery (p) versus the center (c) of the nucleus (n>30 cells per condition). (**C**) Image segments (50 pixels^2) centered on the middle of the nucleus were extracted in both the Sis1-YFP and Cfi1-mKate channels for individual cells (n = 25 cells for both conditions). Images were stacked and average intensity was projected. The Cfi1 ring under control conditions results from the composite of images: in most cells it appears localized to one side, but always at the periphery of the nucleus. Fluorescent line scans quantify the localization patterns. (**D**) Micrographs of cells expressing Hsp104-mKate were imaged live in untreated conditions or after DZA treatment (5 µg/ml, 30 min). Below micrographs, quantification of number of Hsp104 foci and Sis1 peripheral localization (n>30 cells/condition).

bioRxiv preprint doi: https://doi.org/10.1101/458810; this version posted October 31, 2018. The copyright holder for this preprint (which was not certified by peer review) is the author/funder. All rights reserved. No reuse allowed without permission.

Figure 6

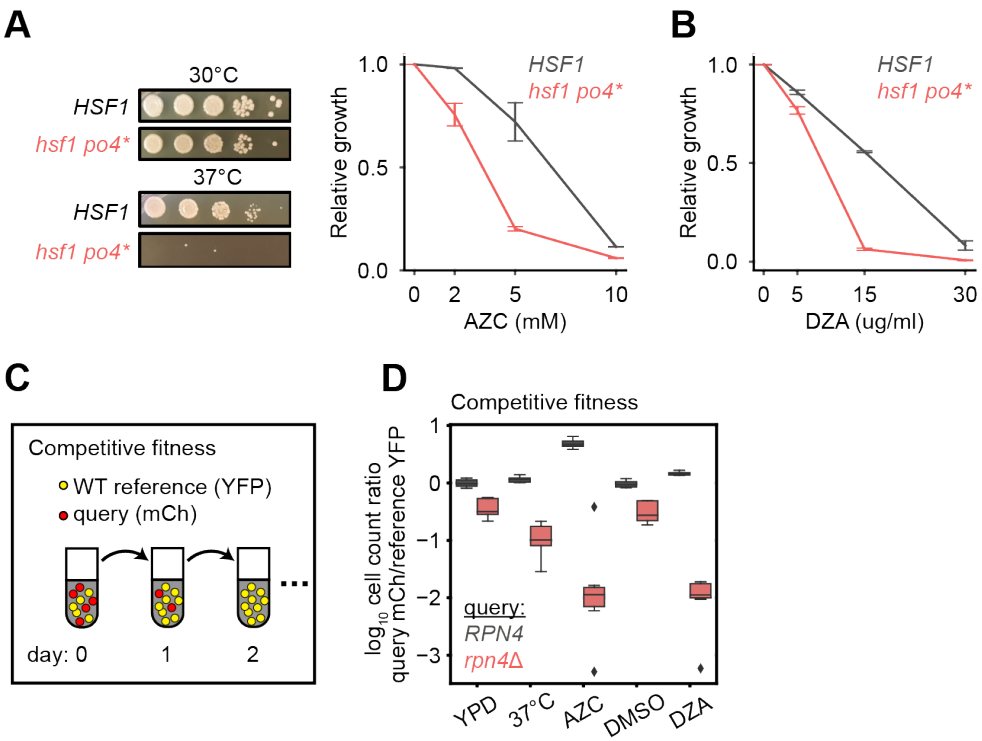

Figure 6. Hsf1 and Rpn4 support cell fitness under RPAS. (**A**) Growth defects of *hsf1 po4** cells. Left panels, wild type (*HSF1)* and mutant (*hsf1 po4**, all serine to aspartate) cells were serially diluted 1:10 onto YPD plates and incubated at 30 or 37°C for 2 days. Right panel, cells were grown for 24 h in the presence of the indicated concentration of AZC and relative growth (compared to untreated) was determined by OD_{600}. Line represents the average and error bars the range of n=2 biological replicates. (**B**) Cells were grown for 24 h in the presence of the indicated concentration of DZA and relative growth (compared to untreated) was determined by OD_{600}. Line represents the average and error bars the range of n=2 biological replicates. (**C**) Schematic of competitive fitness assay. Wild type cells expressing YFP and query cells expressing mCherry (mCh) were co-cultured in each condition over 5 days. Abundance of YFP+ and mCh+ cells was determined daily by flow cytometry. (**D**) The $\log_{10}$ ratio of mCh+ (query) to YFP+ (WT reference) of wild type (*RPN4*) and *rpn4*Δ cells after 3 days of co-culture in YPD, YPD at 37°C, 5 mM AZC, vehicle (DMSO) and DZA (15 µg/ml) (n=8 biological replicates per condition).

bioRxiv preprint doi: https://doi.org/10.1101/458810; this version posted October 31, 2018. The copyright holder for this preprint (which was not certified by peer review) is the author/funder. All rights reserved. No reuse allowed without permission.

Figure 7

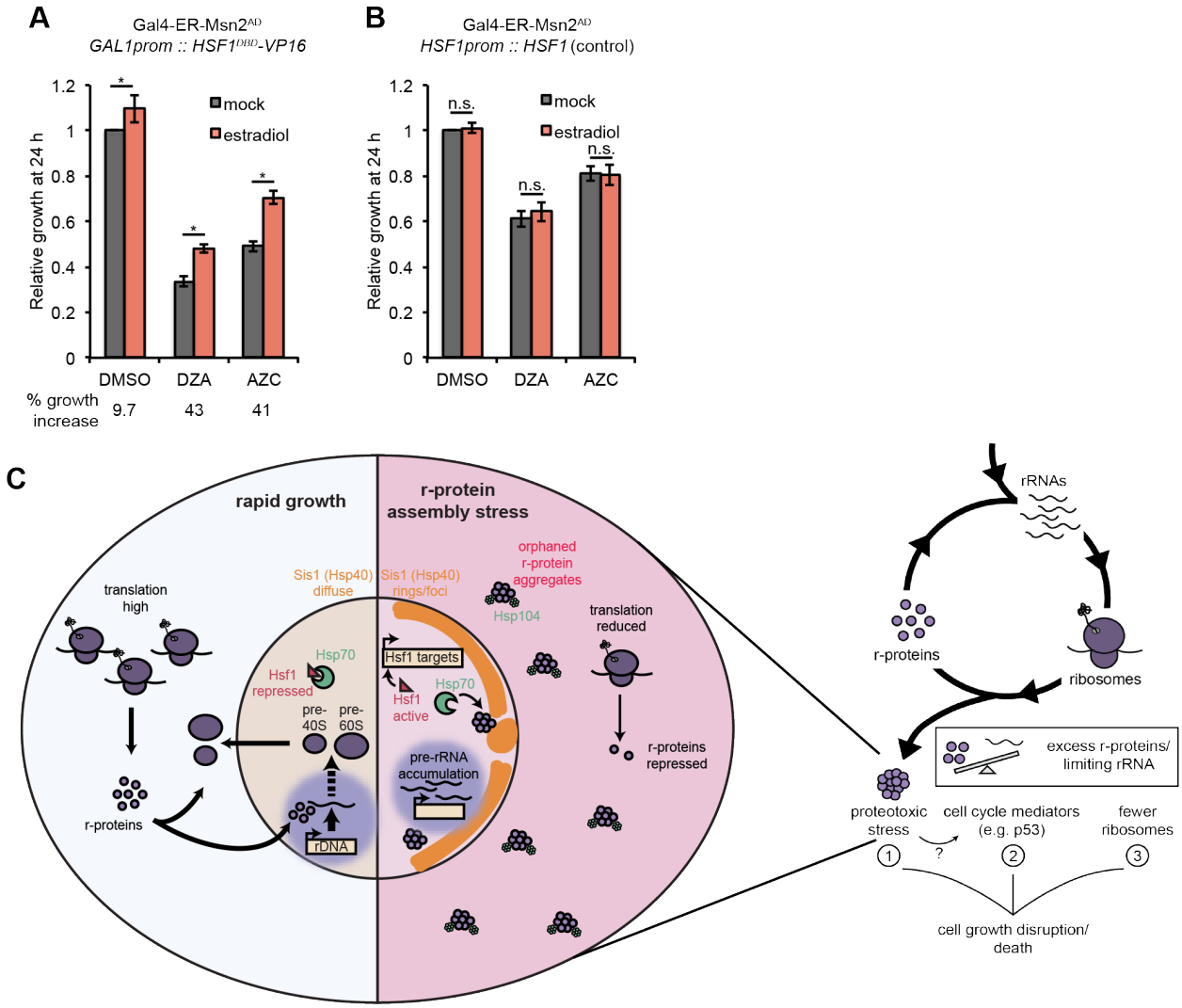

Figure 7. Proteostatic strain contributes to the growth defect of cells under RPAS. (**A**) Growth of cells expressing a synthetic Hsf1 construct severed from negative regulation by chaperones ($Hsf1^{DBD}$-VP16) was expressed under an estradiol-responsive promoter. Pre-conditioning was performed with estradiol (2 nM) for 3 h prior to addition of DMSO, DZA (8 µg/ml), or AZC (2.5 mM) for an additional 21 h. Growth was determined as OD_{600} normalized to DMSO control. Bar height depicts the average and error bars the standard deviation of n=3 biological replicates. Values below indicate the average % increase in growth by estradiol pre-conditioning versus mock. *, all $p<0.01$ (Student's t-test). (**B**) Results of experiments performed identically as described in A, but with an isogenic strain containing *HSF1* under its WT promoter instead of the $Hsf1^{DBD}$-VP16 under an estradiol-responsive promoter. n.s., not significant, all $p>0.1$ (Student's t-test). (**C**) Model of how disruptions to ribosome biogenesis leads to RPAS and the impacts on cellular physiology. During proliferation, cells rapidly produce ribosomes through coordinated synthesis of r-proteins (purple circles) in the cytoplasm and rRNAs in the nucleolus. Perturbations that result in orphan r-proteins result in proteotoxic stress following r-protein aggregation (left panel). In the cytoplasm, aggregates are visible via Hsp104 foci and translation is downregulated. In the nucleus, Hsp40 Sis1 (orange), and possibly Hsp70, are targeted to aggregates and the nucleolus moves from the nuclear periphery, to adjacent to Sis1-marked "rings". Concomitantly, pre-rRNA accumulates, r-protein genes are transcriptionally repressed, and Hsf1 is liberated from Hsp70 sequestration to activate target genes encoding protein folding and degradation machinery. Proteostasis collapse stalls growth independently from reduced pools of ribosomes (right panel).

bioRxiv preprint doi: https://doi.org/10.1101/458810; this version posted October 31, 2018. The copyright holder for this preprint (which was not certified by peer review) is the author/funder. All rights reserved. No reuse allowed without permission.

References:

Acosta-Alvear, D., Cho, M.Y., Wild, T., Buchholz, T.J., Lerner, A.G., Simakova, O., Hahn, J., Korde, N., Landgren, O., Maric, I., et al. (2015). Paradoxical resistance of multiple myeloma to proteasome inhibitors by decreased levels of 19S proteasomal subunits. Elife *4*, e08153.

Akerfelt, M., Morimoto, R.I., and Sistonen, L. (2010). Heat shock factors: integrators of cell stress, development and lifespan. Nat. Rev. Mol. Cell Biol. *11*, 545–555.

Amsterdam, A., Sadler, K.C., Lai, K., Farrington, S., Bronson, R.T., Lees, J.A., and Hopkins, N. (2004). Many ribosomal protein genes are cancer genes in zebrafish. PLoS Biol. *2*, E139.

Arlet, J.-B., Ribeil, J.-A., Guillem, F., Negre, O., Hazoume, A., Marcion, G., Beuzard, Y., Dussiot, M., Moura, I.C., Demarest, S., et al. (2014). HSP70 sequestration by free α-globin promotes ineffective erythropoiesis in β-thalassaemia. Nature *514*, 242–246.

Balch, W.E., Morimoto, R.I., Dillin, A., and Kelly, J.W. (2008). Adapting proteostasis for disease intervention. Science *319*, 916–919.

Boulon, S., Westman, B.J., Hutten, S., Boisvert, F.-M., and Lamond, A.I. (2010). The nucleolus under stress. Mol. Cell *40*, 216–227.

Brandman, O., Stewart-Ornstein, J., Wong, D., Larson, A., Williams, C.C., Li, G.-W., Zhou, S., King, D., Shen, P.S., Weibezahn, J., et al. (2012). A ribosome-bound quality control complex triggers degradation of nascent peptides and signals translation stress. Cell *151*, 1042–1054.

Breslow, D.K., Cameron, D.M., Collins, S.R., Schuldiner, M., Stewart-Ornstein, J., Newman, H.W., Braun, S., Madhani, H.D., Krogan, N.J., and Weissman, J.S. (2008). A comprehensive strategy enabling high-resolution functional analysis of the yeast genome. Nat. Methods *5*, 711–718.

Burger, K., Mühl, B., Harasim, T., Rohrmoser, M., Malamoussi, A., Orban, M., Kellner, M., Gruber-Eber, A., Kremmer, E., Hölzel, M., et al. (2010). Chemotherapeutic drugs inhibit ribosome biogenesis at various levels. J. Biol. Chem. *285*, 12416–12425.

Churchman, L.S., and Weissman, J.S. (2011). Nascent transcript sequencing visualizes transcription at nucleotide resolution. Nature *469*, 368–373.

Cloutier, S.C., Wang, S., Ma, W.K., Petell, C.J., and Tran, E.J. (2013). Long noncoding RNAs promote transcriptional poising of inducible genes. PLoS Biol. *11*, e1001715.

Couvillion, M.T., Soto, I.C., Shipkovenska, G., and Churchman, L.S. (2016). Synchronized mitochondrial and cytosolic translation programs. Nature *533*, 499–503.

David, D.C., Ollikainen, N., Trinidad, J.C., Cary, M.P., Burlingame, A.L., and Kenyon, C.

bioRxiv preprint doi: https://doi.org/10.1101/458810; this version posted October 31, 2018. The copyright holder for this preprint (which was not certified by peer review) is the author/funder. All rights reserved. No reuse allowed without permission.

(2010). Widespread protein aggregation as an inherent part of aging in C. elegans. PLoS Biol. *8*, e1000450.

Dephoure, N., Hwang, S., O'Sullivan, C., Dodgson, S.E., Gygi, S.P., Amon, A., and Torres, E.M. (2014). Quantitative proteomic analysis reveals posttranslational responses to aneuploidy in yeast. Elife *3*, e03023.

Dever, T.E., Feng, L., Wek, R.C., Cigan, A.M., Donahue, T.F., and Hinnebusch, A.G. (1992). Phosphorylation of initiation factor 2 alpha by protein kinase GCN2 mediates gene-specific translational control of GCN4 in yeast. Cell *68*, 585–596.

Draptchinskaia, N., Gustavsson, P., Andersson, B., Pettersson, M., Willig, T.N., Dianzani, I., Ball, S., Tchernia, G., Klar, J., Matsson, H., et al. (1999). The gene encoding ribosomal protein S19 is mutated in Diamond-Blackfan anaemia. Nat. Genet. *21*, 169–175.

El Hage, A., Koper, M., Kufel, J., and Tollervey, D. (2008). Efficient termination of transcription by RNA polymerase I requires the 5' exonuclease Rat1 in yeast. Genes Dev. *22*, 1069–1081.

Fang, N.N., Chan, G.T., Zhu, M., Comyn, S.A., Persaud, A., Deshaies, R.J., Rotin, D., Gsponer, J., and Mayor, T. (2014). Rsp5/Nedd4 is the main ubiquitin ligase that targets cytosolic misfolded proteins following heat stress. Nat. Cell Biol. *16*, 1227–1237.

Fleming, J.A., Lightcap, E.S., Sadis, S., Thoroddsen, V., Bulawa, C.E., and Blackman, R.K. (2002). Complementary whole-genome technologies reveal the cellular response to proteasome inhibition by PS-341. Proc. Natl. Acad. Sci. U. S. A. *99*, 1461–1466.

Gasch, A.P., Spellman, P.T., Kao, C.M., Carmel-Harel, O., Eisen, M.B., Storz, G., Botstein, D., and Brown, P.O. (2000). Genomic expression programs in the response of yeast cells to environmental changes. Mol. Biol. Cell *11*, 4241–4257.

Geiler-Samerotte, K.A., Dion, M.F., Budnik, B.A., Wang, S.M., Hartl, D.L., and Drummond, D.A. (2011). Misfolded proteins impose a dosage-dependent fitness cost and trigger a cytosolic unfolded protein response in yeast. Proceedings of the National Academy of Sciences *108*, 680–685.

Gietz, R.D., and Schiestl, R.H. (2007). High-efficiency yeast transformation using the LiAc/SS carrier DNA/PEG method. Nat. Protoc. *2*, 31–34.

Glover, J.R., and Lindquist, S. (1998). Hsp104, Hsp70, and Hsp40: a novel chaperone system that rescues previously aggregated proteins. Cell *94*, 73–82.

González, A., Shimobayashi, M., Eisenberg, T., Merle, D.A., Pendl, T., Hall, M.N., and Moustafa, T. (2015). TORC1 promotes phosphorylation of ribosomal protein S6 via the AGC kinase Ypk3 in Saccharomyces cerevisiae. PLoS One *10*, e0120250.

bioRxiv preprint doi: https://doi.org/10.1101/458810; this version posted October 31, 2018. The copyright holder for this preprint (which was not certified by peer review) is the author/funder. All rights reserved. No reuse allowed without permission.

Goudarzi, K.M., and Lindström, M.S. (2016). Role of ribosomal protein mutations in tumor development (Review). Int. J. Oncol. *48*, 1313–1324.

Gsponer, J., and Babu, M.M. (2012). Cellular strategies for regulating functional and nonfunctional protein aggregation. Cell Rep. *2*, 1425–1437.

Guimaraes, J.C., and Zavolan, M. (2016). Patterns of ribosomal protein expression specify normal and malignant human cells. Genome Biol. *17*, 236.

Haruki, H., Nishikawa, J., and Laemmli, U.K. (2008). The anchor-away technique: rapid, conditional establishment of yeast mutant phenotypes. Mol. Cell *31*, 925–932.

Hill, S.M., Hanzén, S., and Nyström, T. (2017). Restricted access: spatial sequestration of damaged proteins during stress and aging. EMBO Rep. *18*, 377–391.

Holmes, W.M., Klaips, C.L., and Serio, T.R. (2014). Defining the limits: Protein aggregation and toxicity in vivo. Crit. Rev. Biochem. Mol. Biol. *49*, 294–303.

Jäkel, S., Mingot, J.-M., Schwarzmaier, P., Hartmann, E., and Görlich, D. (2002). Importins fulfil a dual function as nuclear import receptors and cytoplasmic chaperones for exposed basic domains. EMBO J. *21*, 377–386.

James, A., Wang, Y., Raje, H., Rosby, R., and DiMario, P. (2014). Nucleolar stress with and without p53. Nucleus *5*, 402–426.

Jorgensen, P., Rupes, I., Sharom, J.R., Schneper, L., Broach, J.R., and Tyers, M. (2004). A dynamic transcriptional network communicates growth potential to ribosome synthesis and critical cell size. Genes Dev. *18*, 2491–2505.

Joshi, S., Wang, T., Araujo, T.L.S., Sharma, S., Brodsky, J.L., and Chiosis, G. (2018). Adapting to stress - chaperome networks in cancer. Nat. Rev. Cancer *18*, 562–575.

Kaganovich, D., Kopito, R., and Frydman, J. (2008). Misfolded proteins partition between two distinct quality control compartments. Nature *454*, 1088–1095.

Kapitzky, L., Beltrao, P., Berens, T.J., Gassner, N., Zhou, C., Wüster, A., Wu, J., Babu, M.M., Elledge, S.J., Toczyski, D., et al. (2010). Cross-species chemogenomic profiling reveals evolutionarily conserved drug mode of action. Mol. Syst. Biol. *6*, 451.

Khajuria, R.K., Munschauer, M., Ulirsch, J.C., Fiorini, C., Ludwig, L.S., McFarland, S.K., Abdulhay, N.J., Specht, H., Keshishian, H., Mani, D.R., et al. (2018). Ribosome Levels Selectively Regulate Translation and Lineage Commitment in Human Hematopoiesis. Cell *173*, 90–103.e19.

Koplin, A., Preissler, S., Ilina, Y., Koch, M., Scior, A., Erhardt, M., and Deuerling, E. (2010). A dual function for chaperones SSB-RAC and the NAC nascent polypeptide-associated

bioRxiv preprint doi: https://doi.org/10.1101/458810; this version posted October 31, 2018. The copyright holder for this preprint (which was not certified by peer review) is the author/funder. All rights reserved. No reuse allowed without permission.

complex on ribosomes. J. Cell Biol. *189*, 57–68.

Kos-Braun, I.C., Jung, I., and Koš, M. (2017). Tor1 and CK2 kinases control a switch between alternative ribosome biogenesis pathways in a growth-dependent manner. PLoS Biol. *15*, e2000245.

Kressler, D., Bange, G., Ogawa, Y., Stjepanovic, G., Bradatsch, B., Pratte, D., Amlacher, S., Strauß, D., Yoneda, Y., Katahira, J., et al. (2012). Synchronizing nuclear import of ribosomal proteins with ribosome assembly. Science *338*, 666–671.

Kressler, D., Hurt, E., and Baßler, J. (2017). A Puzzle of Life: Crafting Ribosomal Subunits. Trends Biochem. Sci. *42*, 640–654.

Kushnirov, V.V. (2000). Rapid and reliable protein extraction from yeast. Yeast *16*, 857–860.

Kusmierczyk, A.R., Kunjappu, M.J., Funakoshi, M., and Hochstrasser, M. (2008). A multimeric assembly factor controls the formation of alternative 20S proteasomes. Nat. Struct. Mol. Biol. *15*, 237–244.

Lam, Y.W., Lamond, A.I., Mann, M., and Andersen, J.S. (2007). Analysis of nucleolar protein dynamics reveals the nuclear degradation of ribosomal proteins. Curr. Biol. *17*, 749–760.

Lempiäinen, H., and Shore, D. (2009). Growth control and ribosome biogenesis. Curr. Opin. Cell Biol. *21*, 855–863.

Liu, Y., Liang, S., and Tartakoff, A.M. (1996). Heat shock disassembles the nucleolus and inhibits nuclear protein import and poly(A)+ RNA export. EMBO J. *15*, 6750–6757.

Loibl, M., Klein, I., Prattes, M., Schmidt, C., Kappel, L., Zisser, G., Gungl, A., Krieger, E., Pertschy, B., and Bergler, H. (2014). The drug diazaborine blocks ribosome biogenesis by inhibiting the AAA-ATPase Drg1. J. Biol. Chem. *289*, 3913–3922.

Love, M.I., Huber, W., and Anders, S. (2014). Moderated estimation of fold change and dispersion for RNA-seq data with DESeq2. Genome Biol. *15*, 550.

Marion, R.M., Regev, A., Segal, E., Barash, Y., Koller, D., Friedman, N., and O'Shea, E.K. (2004). Sfp1 is a stress- and nutrient-sensitive regulator of ribosomal protein gene expression. Proc. Natl. Acad. Sci. U. S. A. *101*, 14315–14322.

Mayer, C., and Grummt, I. (2006). Ribosome biogenesis and cell growth: mTOR coordinates transcription by all three classes of nuclear RNA polymerases. Oncogene *25*, 6384–6391.

McShane, E., Sin, C., Zauber, H., Wells, J.N., Donnelly, N., Wang, X., Hou, J., Chen, W., Storchova, Z., Marsh, J.A., et al. (2016). Kinetic Analysis of Protein Stability Reveals Age-Dependent Degradation. Cell *167*, 803–815.e21.

Medicherla, B., and Goldberg, A.L. (2008). Heat shock and oxygen radicals stimulate

bioRxiv preprint doi: https://doi.org/10.1101/458810; this version posted October 31, 2018. The copyright holder for this preprint (which was not certified by peer review) is the author/funder. All rights reserved. No reuse allowed without permission.

ubiquitin-dependent degradation mainly of newly synthesized proteins. J. Cell Biol. *182*, 663–673.

Miller, S.B.M., Ho, C.-T., Winkler, J., Khokhrina, M., Neuner, A., Mohamed, M.Y.H., Guilbride, D.L., Richter, K., Lisby, M., Schiebel, E., et al. (2015a). Compartment-specific aggregases direct distinct nuclear and cytoplasmic aggregate deposition. EMBO J. *34*, 778–797.

Miller, S.B.M., Mogk, A., and Bukau, B. (2015b). Spatially organized aggregation of misfolded proteins as cellular stress defense strategy. J. Mol. Biol. *427*, 1564–1574.

Mills, E.W., and Green, R. (2017). Ribosomopathies: There's strength in numbers. Science *358*.

Moqtaderi, Z., and Struhl, K. (2008). Expanding the repertoire of plasmids for PCR-mediated epitope tagging in yeast. Yeast *25*, 287–292.

Narla, A., and Ebert, B.L. (2010). Ribosomopathies: human disorders of ribosome dysfunction. Blood *115*, 3196–3205.

Nishimura, K., Fukagawa, T., Takisawa, H., Kakimoto, T., and Kanemaki, M. (2009). An auxin-based degron system for the rapid depletion of proteins in nonplant cells. Nat. Methods *6*, 917–922.

Olzscha, H., Schermann, S.M., Woerner, A.C., Pinkert, S., Hecht, M.H., Tartaglia, G.G., Vendruscolo, M., Hayer-Hartl, M., Hartl, F.U., and Vabulas, R.M. (2011). Amyloid-like aggregates sequester numerous metastable proteins with essential cellular functions. Cell *144*, 67–78.

Pakos-Zebrucka, K., Koryga, I., Mnich, K., Ljujic, M., Samali, A., and Gorman, A.M. (2016). The integrated stress response. EMBO Rep. *17*, 1374–1395.

Park, S.-H., Kukushkin, Y., Gupta, R., Chen, T., Konagai, A., Hipp, M.S., Hayer-Hartl, M., and Hartl, F.U. (2013). PolyQ proteins interfere with nuclear degradation of cytosolic proteins by sequestering the Sis1p chaperone. Cell *154*, 134–145.

Pelham, H.R. (1984). Hsp70 accelerates the recovery of nucleolar morphology after heat shock. EMBO J. *3*, 3095–3100.

Pelletier, J., Thomas, G., and Volarević, S. (2018). Ribosome biogenesis in cancer: new players and therapeutic avenues. Nat. Rev. Cancer *18*, 51–63.

Pertschy, B., Zisser, G., Schein, H., Köffel, R., Rauch, G., Grillitsch, K., Morgenstern, C., Durchschlag, M., Högenauer, G., and Bergler, H. (2004). Diazaborine treatment of yeast cells inhibits maturation of the 60S ribosomal subunit. Mol. Cell. Biol. *24*, 6476–6487.

Pillet, B., Mitterer, V., Kressler, D., and Pertschy, B. (2017). Hold on to your friends:

bioRxiv preprint doi: https://doi.org/10.1101/458810; this version posted October 31, 2018. The copyright holder for this preprint (which was not certified by peer review) is the author/funder. All rights reserved. No reuse allowed without permission.

Dedicated chaperones of ribosomal proteins: Dedicated chaperones mediate the safe transfer of ribosomal proteins to their site of pre-ribosome incorporation. Bioessays *39*, 1–12.

Pincus, D., Anandhakumar, J., Thiru, P., Guertin, M.J., Erkine, A.M., and Gross, D.S. (2018). Genetic and Epigenetic Determinants Establish a Continuum of Hsf1 Occupancy and Activity Across the Yeast Genome.

Reiter, A., Steinbauer, R., Philippi, A., Gerber, J., Tschochner, H., Milkereit, P., and Griesenbeck, J. (2011). Reduction in ribosomal protein synthesis is sufficient to explain major effects on ribosome production after short-term TOR inactivation in Saccharomyces cerevisiae. Mol. Cell. Biol. *31*, 803–817.

Ruan, L., Zhou, C., Jin, E., Kucharavy, A., Zhang, Y., Wen, Z., Florens, L., and Li, R. (2017). Cytosolic proteostasis through importing of misfolded proteins into mitochondria. Nature *543*, 443–446.

Shalgi, R., Hurt, J.A., Krykbaeva, I., Taipale, M., Lindquist, S., and Burge, C.B. (2013). Widespread regulation of translation by elongation pausing in heat shock. Mol. Cell *49*, 439–452.

Solís, E.J., Pandey, J.P., Zheng, X., Jin, D.X., Gupta, P.B., Airoldi, E.M., Pincus, D., and Denic, V. (2016). Defining the Essential Function of Yeast Hsf1 Reveals a Compact Transcriptional Program for Maintaining Eukaryotic Proteostasis. Mol. Cell *63*, 60–71.

Stefani, M., and Dobson, C.M. (2003). Protein aggregation and aggregate toxicity: new insights into protein folding, misfolding diseases and biological evolution. J. Mol. Med. *81*, 678–699.

Steffen, K.K., MacKay, V.L., Kerr, E.O., Tsuchiya, M., Hu, D., Fox, L.A., Dang, N., Johnston, E.D., Oakes, J.A., Tchao, B.N., et al. (2008). Yeast life span extension by depletion of 60s ribosomal subunits is mediated by Gcn4. Cell *133*, 292–302.

Steffen, K.K., McCormick, M.A., Pham, K.M., MacKay, V.L., Delaney, J.R., Murakami, C.J., Kaeberlein, M., and Kennedy, B.K. (2012). Ribosome deficiency protects against ER stress in Saccharomyces cerevisiae. Genetics *191*, 107–118.

Stewart-Ornstein, J., Weissman, J.S., and El-Samad, H. (2012). Cellular noise regulons underlie fluctuations in Saccharomyces cerevisiae. Mol. Cell *45*, 483–493.

Summers, D.W., Wolfe, K.J., Ren, H.Y., and Cyr, D.M. (2013). The Type II Hsp40 Sis1 cooperates with Hsp70 and the E3 ligase Ubr1 to promote degradation of terminally misfolded cytosolic protein. PLoS One *8*, e52099.

Sung, M.-K., Porras-Yakushi, T.R., Reitsma, J.M., Huber, F.M., Sweredoski, M.J., Hoelz, A., Hess, S., and Deshaies, R.J. (2016a). A conserved quality-control pathway that mediates degradation of unassembled ribosomal proteins. Elife *5*.

bioRxiv preprint doi: https://doi.org/10.1101/458810; this version posted October 31, 2018. The copyright holder for this preprint (which was not certified by peer review) is the author/funder. All rights reserved. No reuse allowed without permission.

Sung, M.-K., Reitsma, J.M., Sweredoski, M.J., Hess, S., and Deshaies, R.J. (2016b). Ribosomal proteins produced in excess are degraded by the ubiquitin-proteasome system. Mol. Biol. Cell *27*, 2642–2652.

Tkach, J.M., and Glover, J.R. (2004). Amino acid substitutions in the C-terminal AAA+ module of Hsp104 prevent substrate recognition by disrupting oligomerization and cause high temperature inactivation. J. Biol. Chem. *279*, 35692–35701.

Trotter, E.W., Kao, C.M.-F., Berenfeld, L., Botstein, D., Petsko, G.A., and Gray, J.V. (2002). Misfolded proteins are competent to mediate a subset of the responses to heat shock in Saccharomyces cerevisiae. J. Biol. Chem. *277*, 44817–44825.

Tsvetkov, P., Mendillo, M.L., Zhao, J., Carette, J.E., Merrill, P.H., Cikes, D., Varadarajan, M., van Diemen, F.R., Penninger, J.M., Goldberg, A.L., et al. (2015). Compromising the 19S proteasome complex protects cells from reduced flux through the proteasome. eLife Sciences *4*, e08467.

Turowski, T.W., and Tollervey, D. (2015). Cotranscriptional events in eukaryotic ribosome synthesis. Wiley Interdiscip. Rev. RNA *6*, 129–139.

Urban, J., Soulard, A., Huber, A., Lippman, S., Mukhopadhyay, D., Deloche, O., Wanke, V., Anrather, D., Ammerer, G., Riezman, H., et al. (2007). Sch9 is a major target of TORC1 in Saccharomyces cerevisiae. Mol. Cell *26*, 663–674.

Wallace, E.W.J., Kear-Scott, J.L., Pilipenko, E.V., Schwartz, M.H., Laskowski, P.R., Rojek, A.E., Katanski, C.D., Riback, J.A., Dion, M.F., Franks, A.M., et al. (2015). Reversible, Specific, Active Aggregates of Endogenous Proteins Assemble upon Heat Stress. Cell *162*, 1286–1298.

Wang, F., Chan, C., Weir, N.R., and Denic, V. (2014). The Get1/2 transmembrane complex is an endoplasmic-reticulum membrane protein insertase. Nature *512*, 441–444.

Wang, J., Atolia, E., Hua, B., Savir, Y., Escalante-Chong, R., and Springer, M. (2015). Natural variation in preparation for nutrient depletion reveals a cost-benefit tradeoff. PLoS Biol. *13*, e1002041.

Wang, X., Xu, H., Ju, D., and Xie, Y. (2008). Disruption of Rpn4-induced proteasome expression in Saccharomyces cerevisiae reduces cell viability under stressed conditions. Genetics *180*, 1945–1953.

Wang, X., Xu, H., Ha, S.-W., Ju, D., and Xie, Y. (2010). Proteasomal degradation of Rpn4 in Saccharomyces cerevisiae is critical for cell viability under stressed conditions. Genetics *184*, 335–342.

Warner, J.R. (1999). The economics of ribosome biosynthesis in yeast. Trends Biochem. Sci. *24*, 437–440.

bioRxiv preprint doi: https://doi.org/10.1101/458810; this version posted October 31, 2018. The copyright holder for this preprint (which was not certified by peer review) is the author/funder. All rights reserved. No reuse allowed without permission.

Weidberg, H., and Amon, A. (2018). MitoCPR-A surveillance pathway that protects mitochondria in response to protein import stress. Science *360*.

Wek, R.C. (2018). Role of eIF2α Kinases in Translational Control and Adaptation to Cellular Stress. Cold Spring Harb. Perspect. Biol. *10*.

Wendler, F., Bergler, H., Prutej, K., Jungwirth, H., Zisser, G., Kuchler, K., and Högenauer, G. (1997). Diazaborine Resistance in the Yeast Saccharomyces cerevisiae Reveals a Link between YAP1 and the Pleiotropic Drug Resistance Genes PDR1 andPDR3. J. Biol. Chem. *272*, 27091–27098.

Woolford, J.L., and Baserga, S.J. (2013). Ribosome Biogenesis in the Yeast Saccharomyces cerevisiae. Genetics *195*, 643–681.

Wrobel, L., Topf, U., Bragoszewski, P., Wiese, S., Sztolsztener, M.E., Oeljeklaus, S., Varabyova, A., Lirski, M., Chroscicki, P., Mroczek, S., et al. (2015). Mistargeted mitochondrial proteins activate a proteostatic response in the cytosol. Nature *524*, 485–488.

Yoneda, T., Benedetti, C., Urano, F., Clark, S.G., Harding, H.P., and Ron, D. (2004). Compartment-specific perturbation of protein handling activates genes encoding mitochondrial chaperones. J. Cell Sci. *117*, 4055–4066.

Zheng, X., Krakowiak, J., Patel, N., Beyzavi, A., Ezike, J., Khalil, A.S., and Pincus, D. (2016). Dynamic control of Hsf1 during heat shock by a chaperone switch and phosphorylation. Elife *5*.

Zhou, C., Slaughter, B.D., Unruh, J.R., Guo, F., Yu, Z., Mickey, K., Narkar, A., Ross, R.T., McClain, M., and Li, R. (2014). Organelle-based aggregation and retention of damaged proteins in asymmetrically dividing cells. Cell *159*, 530–542.

bioRxiv preprint doi: https://doi.org/10.1101/458810; this version posted October 31, 2018. The copyright holder for this preprint (which was not certified by peer review) is the author/funder. All rights reserved. No reuse allowed without permission.

Methods:

Yeast strain construction and growth

Strains were constructed by standard transformation techniques (Gietz and Schiestl, 2007). Gene tagging and deletion was carried out using PCR products or integrating plasmids, and transformants were verified by colony PCR and western blotting where relevant. The Hsf1 activity reporters contain four Hsf1 binding sites (heat shock element, HSE) upstream of a reporter gene (Brandman et al., 2012; Zheng et al., 2016). The *HSE-GFP* and *HSE-mVenus* reporters were integrated at *URA3* and *LEU2*, respectively, and were used interchangeably depending on experimental requirements. *OsTIR1* driven by the *GPD1* promoter was integrated at *LEU2*. The AID tag was added to a *TIR1*-containing strain by transformation with the *V5-IAA7::KANMX6* cassette. Further transformation of AID strains often resulted in loss of *Os*TIR1 activity, reflected by failure to deplete the tagged protein in auxin; accordingly, such transformations were not performed. The *DRG1* and *DRG1*^{V725E} strains were constructed in a diploid by deletion of one *DRG1* allele followed by transformation with the WT or mutant allele on a *URA3*-marked CEN/ARS plasmid (see "Cloning"). Clones containing only the plasmid-borne copy were isolated by sporulation and tetrad dissection. Estradiol-inducible expression strains were generated with a plasmid containing the V5-tagged ORF downstream of the *GAL1* promoter that integrates at *HIS3* in a background expressing the Gal4-ER-Msn2^{AD} transcription factor (Stewart-Ornstein et al., 2012). All strains and plasmids are listed in Tables S1 and S2, respectively.

All experiments were performed at 30°C with cultures were grown in standard YPD (1% yeast extract, 2% peptone, 2% dextrose, pH 5.5) medium unless indicated otherwise. Where indicated, SCD (0.2% synthetic complete amino acids [Sunrise], 0.5% ammonium sulfate, 0.17% yeast nitrogen base, 2% dextrose, pH 5.5) medium was used. Heat shock was performed by adding an equal volume of 44°C media to the culture and immediately shifting to a 37°C incubator.

Drug treatments

Treatments were generally carried out in log-phase cultures at OD ~0.4–0.6, depending on the length of treatment, such that cultures remained in log growth during the course of the experiment. For drugs dissolved in DMSO, vehicle-only controls contained the same final volume of DMSO. Auxin (indole-3-acetic acid, Sigma-Aldrich) was prepared fresh daily at 100 mM in ethanol and added at a final concentration of 100 µM. Diazaborine (DZA, Calbiochem) was prepared at 15 mg/ml in DMSO (stored at -20°C, protected from light) and used at the indicated concentration. Cycloheximide (Sigma-Aldrich) was purchased as a 100 mg/ml DMSO stock and added at a final concentration of 100 µg/ml (for sucrose gradients) or 200 µg/ml (for stress experiments). AZC (L-azetidine-2-carboxylic acid, Sigma-Aldrich) was prepared at 1 M in water and used at the indicated concentration. Diamide (Sigma-Aldrich) was prepared at 1 M in water and added at a final concentration of 1.5 mM. Rapamycin (LC Laboratories) was prepared fresh daily in ethanol and used at a final concentration of 200 ng/ml (to inhibit r-protein synthesis) or 1 µg/ml (for anchor-away, in a rapamycin-resistant

bioRxiv preprint doi: https://doi.org/10.1101/458810; this version posted October 31, 2018. The copyright holder for this preprint (which was not certified by peer review) is the author/funder. All rights reserved. No reuse allowed without permission.

tor1-1 background). Beta-estradiol (Sigma-Aldrich) was prepared as a 1000X stock for each experiment in ethanol and added to the indicated final concentration.

Cloning

DRG1, including promoter and terminator regions, was PCR amplified from genomic DNA with tails containing *Bam*HI and *Not*I sites and cloned into pBluescript KS. The *DRG1*^{V725E} mutant was constructed by Q5 site-directed mutagenesis. WT and mutant were subcloned using the same restriction sites into pRS316 (*URA3* CEN/ARS) and verified by sequencing of the full insert. V5-tagged ORFs were ordered as gBlocks (IDT) with a C-terminal 6xGly-V5 tag and *Xho*I and *Not*I sites and cloned into pNH603 under the *GAL1* promoter. RP ORFs had the sequence of the genomic locus and *GFP* encoded enhanced monomeric GFP (F64L, S65T, A206K).

Total protein extraction and western blotting

Each western blot was repeated a minimum of twice and a representative image is shown in figures. Protein extraction was adapted from the alkaline lysis method(Kushnirov, 2000). One milliliter of a mid-log culture was harvested in a microfuge, aspirated to remove supernatant, and snap-frozen on liquid nitrogen. Pellets were resuspended at RT in 50 µl 100 mM NaOH. After 3 min, 50 µl 2X SDS buffer (4% SDS, 200 mM DTT, 100 mM Tris pH 7.0, 20% glycerol) was added, and the cells were lysed on a heat block for 3 min at 95°C. Cell debris was cleared by centrifugation at 20,000 *g* for 5 min.

Extracts were resolved on NuPAGE Bis-Tris gels (Invitrogen), transferred to nitrocellulose on a Trans-Blot Turbo (Bio-Rad), and blocked in 5% milk/TBST (0.1% Tween-20). AID-tagged and V5-tagged proteins were detected with mouse anti-V5 (Invitrogen, R960-25, 1:2,000). Pgk1 was detected using mouse anti-Pgk1 (Abcam, ab113687, 1:10,000). Rpb1 was detected with rabbit anti-Rpb1 (y-80, Santa Cruz Biotechnology, sc-25758, 1:1,000). Hsp104 was detected with rabbit anti-Hsp104 (Enzo Life Sciences, ADI-SPA-1040, 1:1,000). Hsp70 was detected with mouse anti-Hsp70 (3A3, Abcam, ab5439, 1:1,000). Rps6 phosphorylated at Ser235/236 was detected with rabbit anti-phos-Rps6 (D57.2.2E, Cell Signaling Technology, 1:2,000). eIF2α phosphorylated at Ser51 was detected with rabbit anti-phos-eIF2α (Invitrogen, 44-728G, 1:1,000). Pgk1 and Rpb1 were used as loading controls. Cy3-labeled secondary antibodies were used, and immunoreactive bands were imaged on a Typhoon.

Total RNA extraction and Northern blotting

Each Northern blot was repeated a minimum of twice and a representative image is shown in figures. Two milliliters of a mid-log culture were harvested in a microfuge, aspirated to remove supernatant, and snap-frozen on liquid nitrogen. RNA was extracted by the hot acid-phenol method and ethanol precipitated. RNA purity and concentration were determined on a NanoDrop.

Typically 5 µl (5 µg) of RNA was mixed with 16 µl sample buffer (10 µl formamide, 3.25 µl formaldehyde, 1 µl 20X MOPS, 1 µl 6X DNA loading dye, 0.75 µl 200 µg/ml ethidium

bioRxiv preprint doi: https://doi.org/10.1101/458810; this version posted October 31, 2018. The copyright holder for this preprint (which was not certified by peer review) is the author/funder. All rights reserved. No reuse allowed without permission.

bromide) and denatured for 10 min at 65°C. After chilling briefly on ice, samples were loaded onto a 100 ml 1.2% agarose/1X MOPS gel and electrophoresed for 90 min at 100V in 1X MOPS in a Thermo EasyCast box. Some gels contained 6% formaldehyde and ran for 5 h, but a 90 min run without formaldehyde gave sharper, more even bands. We also found that low EEO agarose gave the best results. RNA integrity and equal loading were examined by imaging ethidium bromide to visualize rRNA bands. RNA was fragmented in the gel for 20 min in 3 M NaCl/10 mM NaOH before downward capillary transfer on a TurboBlotter apparatus using the manufacturer's blotting kit. Transfer ran for 90 min in 3 M NaCl/10 mM NaOH, and then the membrane was UV crosslinked. Pre-5.8S rRNA was resolved by running 1 µg RNA (in 1X TBE-urea loading buffer) on a 6% TBE-urea gel in 0.5X TBE. RNA was electroblotted to a membrane and UV-crosslinked.

RNA was detected with either small DNA oligonucleotides or large (100–500 bp) double-stranded DNA (see Table S3). For oligo probes, the membrane was pre-hybridized at 42°C in ULTRAhyb-Oligo buffer (Thermo Fisher Scientific). The oligo was 5' end–labeled in a reaction containing 25 pmol oligo, 10 U T4 PNK, 2 µl gamma-^{32}P-ATP (PerkinElmer), and 1X PNK buffer. Probe was hybridized overnight and washed twice in 2X SSC/0.5% SDS at 42°C for 30 min before exposure on a phosphor screen and imaging on a Typhoon. For dsDNA probes, the membrane was pre-hybridized at 42°C in 7.5 ml deionized formamide, 3 ml 5 M NaCl, 3 ml 50% dextran sulfate, 1.5 ml 50X Denhardt's, 750 µl 10 mg/ml salmon sperm DNA, 750 µl 1 M Tris 7.5, 75 µl 20% SDS. Probes were made in a reaction containing 50 ng of a PCR product as template, random hexamer primers, Klenow (exo-), and 5 µl alpha-^{32}P-ATP (PerkinElmer). Denatured probes were hybridized overnight and washed twice in 2X SSC/0.5% SDS at 65°C for 30 min before exposure on a phosphor screen and imaging on a Typhoon scanner.

Chromatin immunoprecipitation-quantitative PCR (ChIP-qPCR)

ChIP was performed based off of standard approaches. Fifty milliliters of a mid-log culture were crosslinked in 1% formaldehyde for 30 min at RT and quenched in 125 mM glycine for 10 min. Cells were pelleted and washed twice in ice-cold PBS before snap-freezing on liquid nitrogen. Chromatin was extracted in LB140 (50 mM HEPES pH 7.5, 140 mM NaCl, 1 mM EDTA, 1% Triton X-100, 0.1% sodium deoxycholate, 0.1% SDS and 1X protease inhibitor cocktail [cOmplete EDTA-free, Roche]) by glass bead beating. Chromatin was sonicated to 100–300 bp on a Bioruptor (Diagenode) and diluted 1:10 in WB140 (LB140 without SDS). Diluted chromatin (1.5 ml, corresponding to ~6 ml of the original cell culture volume) was incubated overnight at 4°C with 1 µl rabbit anti-Hsf1 serum (kind gift from Dr. David Gross, Louisiana State University), or normal rabbit serum as a negative control. Twenty-five microliters of washed Protein A Dynabeads (Invitrogen) were added, and the sample was incubated for 4 h. One wash each was performed for 5 min in WB140 (140 mM NaCl), WB500 (500 mM NaCl), WBLiCl (250 mM LiCl), and TE. Samples were eluted from beads in TE/1% SDS and de-crosslinked overnight at 65°C, followed by RNase A and proteinase K treatment and cleanup on columns. Input and IP DNA were quantified using Brilliant III SYBR Green Master Mix (Agilent Technologies) in technical triplicate for each

bioRxiv preprint doi: https://doi.org/10.1101/458810; this version posted October 31, 2018. The copyright holder for this preprint (which was not certified by peer review) is the author/funder. All rights reserved. No reuse allowed without permission.

biological replicate sample. A dilution curve was generated for each input. Data are recorded for each IP as percent of input using Ct values. Primers are available in Table S3.

Protein aggregation assay

Insoluble proteins were isolated using the protocol described in (Wallace et al., 2015). Twenty-five milliliter cultures were grown to mid-log and treated as indicated, pelleted for 1 min at 3,000 *g*, and rinsed once in 1 ml ice-cold WB (20 mM HEPES pH 7.5, 120 mM KCl, 2 mM EDTA). The pellet was re-suspended with 100 µl SPB and dripped into 2 ml safe-lock tubes filled with liquid nitrogen along with a 7 mm stainless steel ball (Retsch). Cells were cryogenically lysed on a Retsch Mixer Mill 400 by four cycles of 90 sec at 30 Hz and re-chilled on liquid nitrogen between each cycle. The grindate was thawed with 400 µl SPB (WB + 0.2 mM DTT + 1X protease inhibitors [cOmplete EDTA-free, Roche] + 1X phosphatase inhibitors [PhosSTOP, Sigma-Aldrich]) for 5 min on ice with repeated flicking and gentle inversion. Where indicated, 2 µl benzonase (Sigma-Aldrich) was included in SPB to degrade RNA and DNA for 10 min on ice. The lysate was clarified for 30 sec at 3,000 *g* to remove cell debris. Twenty microliters of extract was reserved as input. The remaining extract was centrifuged for 20 min at 20,000 *g* to pellet insoluble proteins. The supernatant was decanted and the pellet rinsed with 400 µl ice-cold SPB with brief vortexing and centrifuged again for 20 min. The pellet was re-suspended in 200 µl IPB (8 M urea, 2% SDS, 20 mM HEPES pH 7.5, 150 mM NaCl, 2 mM EDTA, 2 mM DTT, 1X protease inhibitors) at RT. The input was diluted with 160 µl water and 20 µl 100% TCA and precipitated for 10 min on ice, centrifuged for 5 min at 20,000 *g* and washed with 500 µl ice-cold acetone. Inputs were re-suspended in 100 µl IPB. Input and pellet fractions were centrifuged for 5 min at 20,000 *g*, RT. Ten microliters of input (0.5%) and pellet (5%, 10X) were used for western blotting as above.

Sucrose gradient sedimentation

Fifty-milliliter cultures were grown to mid-log and treated as indicated, followed by addition of CHX to 100 µg/ml and incubation for 2 min. All following steps were performed on ice or at 4°C. Cells were pelleted for 2 min at 3,000 *g*, washed once in 10 ml buffer (20 mM Tris pH 7.0, 10 mM $MgCl_2$, 50 mM KCl, 100 µg/ml CHX), and once in 1 ml buffer. Cells were pelleted in a microfuge and snap-frozen on liquid nitrogen. Cells were lysed by addition of 400 µl glass beads and 400 µl lysis buffer (20 mM Tris pH 7.0, 10 mM $MgCl_2$, 50 mM KCl, 100 ug/ml CHX, 1 mM DTT, 50 U/ml SUPERaseIn [Thermo Fisher], 1X protease inhibitors) followed by bead beating for six cycles (1 min on, 2 min off) on ice. Lysate was clarified 10 min at 20,000 *g*. A continuous 12 ml 10–50% sucrose gradient was prepared in 20 mM Tris pH 7.0, 10 mM $MgCl_2$, 50 mM KCl, 100 µg/ml CHX on a BioComp Gradient Station, and 200 µl (~20 A260 units) lysate was layered onto the top and spun for 3 h at 40,000 rpm in a SW41 rotor. Absorbance profiles and fractions were collected on a BioComp Gradient Station.

Competitive fitness and growth assays

Fitness experiments were performed as described(Wang et al., 2015). Query strains (WT and deletions) expressing *TDH3p-mCherry* were co-cultured with a reference strain

bioRxiv preprint doi: https://doi.org/10.1101/458810; this version posted October 31, 2018. The copyright holder for this preprint (which was not certified by peer review) is the author/funder. All rights reserved. No reuse allowed without permission.

expressing *TDH3p-YFP*. All strains were inoculated from single colonies into liquid YPD and grown to saturation. Query and reference strains were mixed 1:1 (v:v) at a total dilution of 1/100 and grown for 6 hours to an OD_{600} of 0.2–0.5. Co-cultured cells were diluted 1/10 to a final OD_{600} of 0.02–0.05 in YPD alone or YPD with: 0.1% (v/v) DMSO (vehicle), 15 µg/mL DZA, 30 µg/mL DZA, or 5 mM AZC and grown at 30°C. Samples were also diluted in YPD and grown at 37°C. Samples were co-cultured for 5 days and diluted 1/100 into fresh media every 24 h. At each time point, an aliquot of each sample was transferred to TE and quantified by flow cytometry on a Stratedigm S1000EX cytometer. Manual segmentation was used to identify the query and reference strain populations. Data are available in Table S5.

To determine relative growth of *HSF1* and *hsf1 po4** (Figures 6A,B) and *DRG1* and *DRG1 V725E* (Figure S3B), overnight cultures were diluted to OD_{600} ~0.05 in the indicated condition, grown for 24 h, and OD_{600} measured. “Relative growth” is the OD_{600} for each condition relative to the vehicle control of that strain.

For estradiol pre-conditioning (Figures 7, S7), overnight cultures grown in SCD were back diluted 1:100 in fresh SCD to ensure mock and estradiol cultures were at the same starting dilution. The culture was immediately split into two flasks (20 ml each), and one was treated with 20 µl 2 µM estradiol (final concentration 2 nM). Mock and estradiol-treated cultures were grown for 3 h and then treated with DMSO (vehicle), 8 µg/ml DZA, or 2.5 mM AZC, grown for an additional 21 h, and OD_{600} measured. “Relative growth” is the OD_{600} for each condition relative to the mock (no estradiol), DMSO only control. Cultures were also assessed for relative cell size distribution by measuring side scatter on a Stratedigm S1000EX cytometer.

Serial dilution plating assay (Figure 6A) was performed by diluting overnight cultures to OD_{600} ~1.0 in fresh media and serially diluting 1:10 on a 96-well plate. The cultures were stamped onto plates using a “frogger” device and grown as indicated.

Thermotolerance (Figure S4) was performed by diluting overnight cultures to OD ~0.05 and growing for 5.5 h. The culture was split and treated with the indicated concentrations of DZA for 45 min. One milliliter was removed and immediately placed on ice as a pre-heat shock control. One milliliter was placed at 50°C for 15 min on a heat block with thorough mixing every 5 min and then placed on ice. Cells were serially diluted 1:10,000 (for pre-heat shock cultures) or 1:100 (for post-heat shock cultures) and 200 µl were spread onto YPD plates. Plates were incubated at 30°C for 2 days and colonies were counted. Reported are the number of colonies formed on each post-heat shock plate, which corresponds to approximately 100,000 cells that were exposed to heat shock as determined from the pre-heat shock plates.

Fluorescence microscopy

Preparing anchor-away strains expressing FRB-GFP–tagged proteins for microscopy was performed as described (Haruki et al., 2008). Briefly, 1 ml of cells was harvested, fixed in 1 ml -20°C methanol for 6 min, and re-suspended in TBS/0.1% Tween with DAPI. Fixed, DAPI-stained cells were spotted onto a 2% agarose pad on a glass slide and topped with a

bioRxiv preprint doi: https://doi.org/10.1101/458810; this version posted October 31, 2018. The copyright holder for this preprint (which was not certified by peer review) is the author/funder. All rights reserved. No reuse allowed without permission.

cover slip. Samples were imaged for both GFP and DAPI on a Nikon Ti2 microscope with a 100x objective and an ORCA-R2 cooled CCD camera (Hamamatsu).

Confocal microscopy of Sis1-YFP, Cfi1-mKate, and Hsp104-mKate was performed live by allowing low density cultures grown in SCD at room temperature to settle in 96-well glass bottom plates coated with concanavalin A. For treatments, medium was removed and fresh SCD containing the indicated drug was added to the well. Imaging was performed on a Nikon Ti microscope with a 100x 1.49 NA objective, a spinning disk confocal setup (Andor Revolution) and an EMCCD camera (Andor).

RNA-seq

RNA was depleted of ribosomal RNA using Yeast Ribo-Zero Gold (Illumina). For all auxin-related experiments, libraries were prepared from biological duplicates (individual strain isolates grown and treated on separate days) using the TruSeq Stranded Kit (Illumina). The diamide RNA-seq data are of libraries were prepared using another RNA-seq library construction protocol, as previously described (Couvillion et al., 2016) and were not done in replicate as the RNA-seq data recapitulated the well-characterized transcriptional response to diamide (Gasch et al., 2000). All libraries were sequenced on an Illumina NextSeq platform.

RNA-seq data analysis

Raw fastq files were processed as follows. The adapter sequence (AGATCGGAAGAG) was removed using Cutadapt (v1.8.3) with option “-m 18” to retain reads >18 nt. Reads were then quality-filtered using PRINSEQ and alignment was performed with TopHat (v2.1.0). The resulting BAM files from each lane on the flow cell were merged, sorted, and indexed with SAMtools. The number of reads for each genomic feature (e.g. transcript), was quantified using HTSeq count. The GTF file was ENSEMBL release 91 for *Saccharomyces cerevisiae*.

Quantification and differential expression for auxin experiments were carried out using DESeq2 (Love et al., 2014) with drug treatment as the variable: two biological replicates each of mock-treated and auxin-treated. RNA abundance changes were reported using the $\log_2$ fold change calculated by DESeq2 for auxin/untreated for each transcript. For +/- diamide datasets, RNA abundance was determined using RPKM and reported as $\log_2$ fold change (diamide vs. untreated) for each transcript.

Transcript classes were defined as follows. Gene lists can be found in Table S4. “Hsf1 targets”: identified using an approach that defines transcripts that fail to be activated when Hsf1 is depleted prior to acute heat shock (Pincus et al., 2018; Solís et al., 2016). “Msn2/4 targets”: classification from (Solís et al., 2016). Plots were generated using only transcripts that were not also in the “Hsf1 target” class. “All others”: all other genes characterized as “Verified ORFs” by SGD, excluding those in “Hsf1 targets” and “Msn2/4 targets” classes. “proteasome subunits”: the 27 genes encoding the 27 subunits of the 26S proteasome. “r-proteins”: the 136 genes encoding the 79 subunits of the ribosome (ribosomal proteins). “other RiBi genes”: 169 unique genes from the SGD GO term “ribosome biogenesis” with r-protein genes removed.

bioRxiv preprint doi: https://doi.org/10.1101/458810; this version posted October 31, 2018. The copyright holder for this preprint (which was not certified by peer review) is the author/funder. All rights reserved. No reuse allowed without permission.

Supplemental Figures:

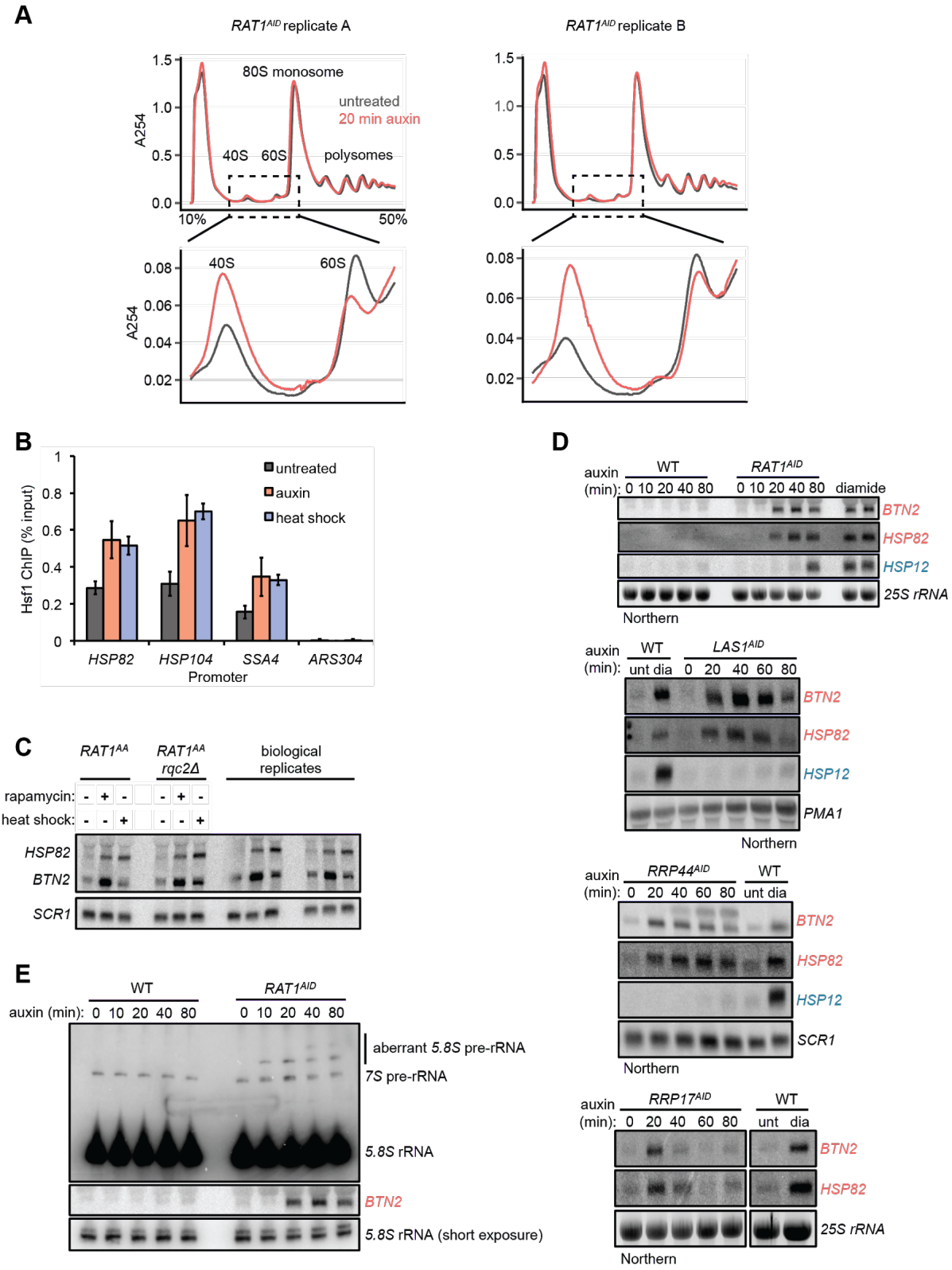

Figure S1. Kinetics of Hsf1 activation. (**A**) Absorbance profiles of sucrose gradients (10-50%) of extracts from *RAT1*^{AID} cells mock or auxin treated for 20 min. Shown are two biological replicates. (**B**) ChIP-qPCR data of Hsf1 at the indicated promoter region of cells untreated, auxin treated, or heat shocked (37°C) for 20 min. Bar

bioRxiv preprint doi: https://doi.org/10.1101/458810; this version posted October 31, 2018. The copyright holder for this preprint (which was not certified by peer review) is the author/funder. All rights reserved. No reuse allowed without permission.

height is the mean and error bars the standard deviation of n=3 biological replicates. (**C**) Rat1 anchor-away cells (see Figure S2) were depleted of Rat1 by rapamycin treatment (1 µg/ml, 40 min) or heat shocked for 20 min. Deletion of *RQC2* did not alter the activation of the Hsf1 targets *HSP82* and *BTN2*. Shown are two biological replicates. (**D**) WT or the indicated AID-tagged strains were treated with auxin for the indicated times and accumulation of Hsf1 targets *HSP82* and *BTN2* and Msn2/4 target *HSP12* was followed by Northern blot. As a control for Hsf1 and Msn2/4 activation, RNA from WT cells untreated or treated with diamide (1.5 mM, 20 min) was included on each blot. RNA was from the same cells used in Figure 1C to allow direct comparison. (**E**) RNA from (D) was probed for pre-5.8S rRNA species (probe 017 (El Hage et al., 2008)). Note that the *BTN2* blot is the same as in (D) and is included for comparison of the kinetics.

bioRxiv preprint doi: https://doi.org/10.1101/458810; this version posted October 31, 2018. The copyright holder for this preprint (which was not certified by peer review) is the author/funder. All rights reserved. No reuse allowed without permission.

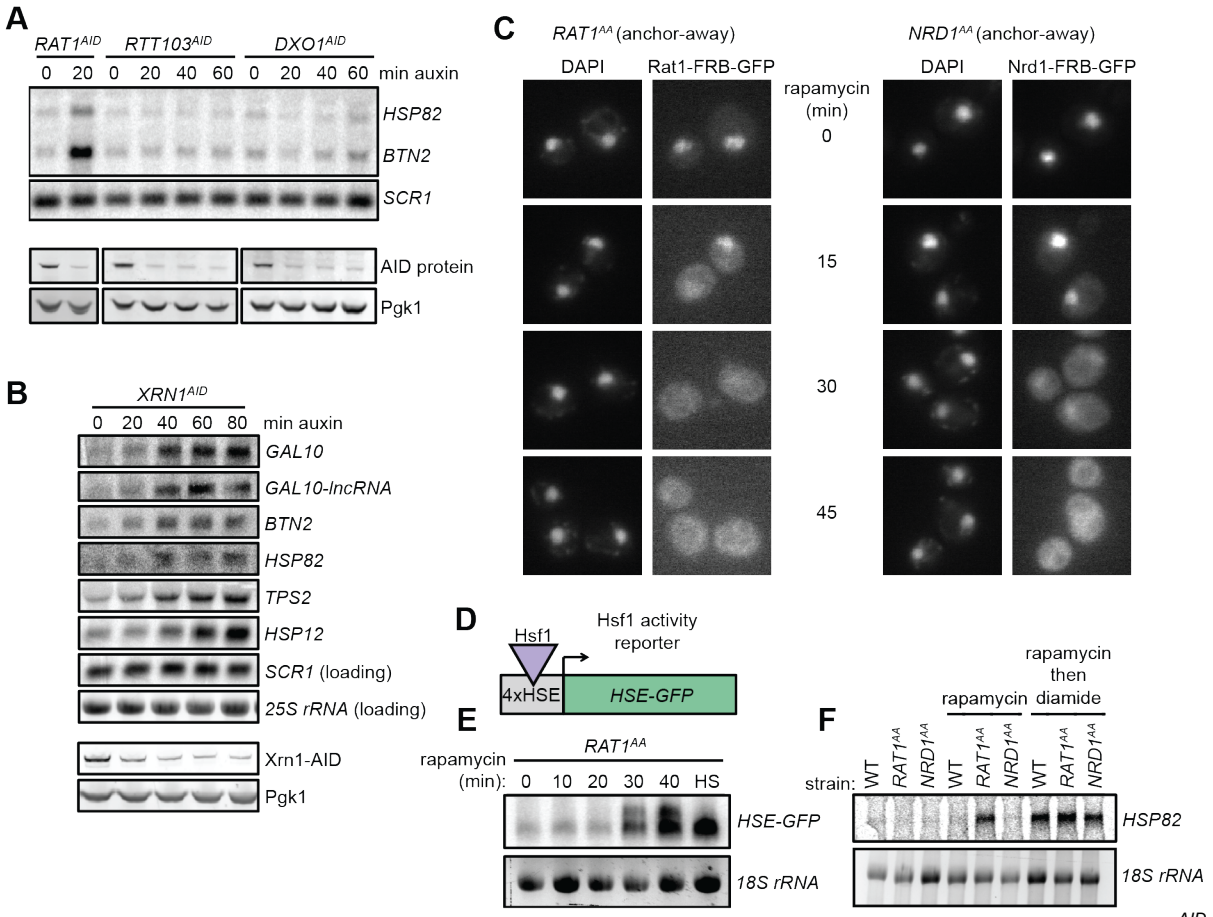

Figure S2. Specificity of Hsf1 activation by depletion of rRNA processing factors. (**A**) *RTT103*^{AID} and *DXO1*^{AID} cells were treated with auxin for the indicated time and assayed for accumulation of Hsf1 targets by Northern. RNA from *RAT1*^{AID} was included as a positive control. Western blots (below) show depletion of AID-tagged proteins. (**B**) *XRN1*^{AID} cells were treated with auxin for the indicated time and the indicated RNAs detected by Northern. Consistent with the role of Xrn1 in RNA turnover, known target transcripts modestly accumulated during the time course of Xrn1 depletion. *GAL10* and *GAL10-lncRNA* are established Xrn1 substrates (Cloutier et al., 2013) that accumulate with kinetics similar to those of Hsf1- (*BTN2* and *HSP82*) and Msn2/4-dependent transcripts (*TPS2* and *HSP12*). Thus, these RNAs accumulated in the absence of normal Xrn1-mediated decay. (**C**) Fluorescence micrographs of Rat1-FRB-GFP and Nrd1-FRB-GFP at indicated time points after rapamycin (1 µg/ml) addition. Nuclei were stained with DAPI. Cell co-express Rpl13a-2xFKBP12 as an anchor and harbor the *tor1-1* mutation, rendering Tor1 insensitive to rapamycin. Addition of rapamycin induces dimerization of FRB-tagged protein to the anchor and rapid nuclear export during export of Rpl13a. (**D**) Schematic of Hsf1 activity reporter transgene *HSE-GFP* consisting of *GFP* driven by four repeats of the Hsf1 binding site (heat shock element, HSE). (**E**) Northern blot for *HSE-GFP* after rapamycin treatment for the indicated time or heat shock (HS, 37°C, 20 min) as a control. (**F**) Northern blot for Hsf1-dependent gene *HSP82* from wild-type or anchor-away strains untreated, treated for 45 min with rapamycin (1 µg/ml), or 45 min rapamycin followed by 20 min diamide (1.5 mM). Nrd1 is a nuclear non-coding RNA transcription termination factor.

bioRxiv preprint doi: https://doi.org/10.1101/458810; this version posted October 31, 2018. The copyright holder for this preprint (which was not certified by peer review) is the author/funder. All rights reserved. No reuse allowed without permission.

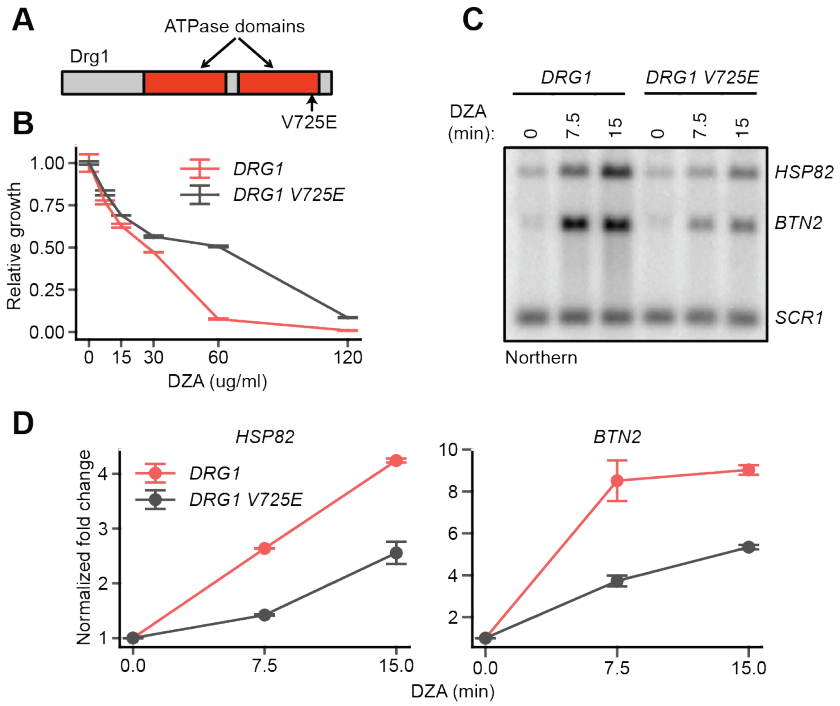

Figure S3. On-target inhibition of Drg1 by DZA. (**A**) Schematic of the yeast Drg1 protein, with the two ATPase domains shown in red. The V725E mutation in the second ATPase domain confers diazaborine resistance (Loibl et al., 2014). (**B**) Growth of WT and *DRG1 V725E* strains after 24 h in the indicated concentration of diazaborine relative to vehicle-only controls. Line indicates the average and error bars the range of n=2 biological replicates. (**C**) Northern blot for Hsf1 target genes in *DRG1 V725E* cells treated with diazaborine (15 µg/ml) for the indicated times. (**D**) Quantification of Northern blots for the indicated Hsf1 target transcripts, normalized against *SCR1*. Line indicates the average and error bars the range of n=2 biological replicates.

bioRxiv preprint doi: https://doi.org/10.1101/458810; this version posted October 31, 2018. The copyright holder for this preprint (which was not certified by peer review) is the author/funder. All rights reserved. No reuse allowed without permission.

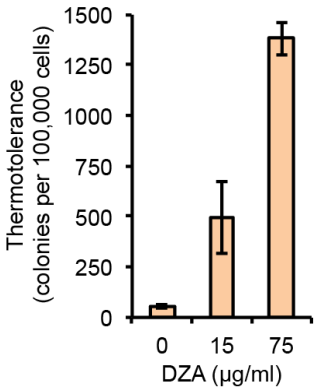

Figure S4. DZA treatment enhances thermotolerance. WT cells treated with the indicated concentration of DZA for 45 min were exposed to 50°C HS for 15 min. Colony forming units were determined from plating approximately 100,000 cells. Bar height depicts the average and error bars the standard deviation of n=3 biological replicates.

bioRxiv preprint doi: https://doi.org/10.1101/458810; this version posted October 31, 2018. The copyright holder for this preprint (which was not certified by peer review) is the author/funder. All rights reserved. No reuse allowed without permission.

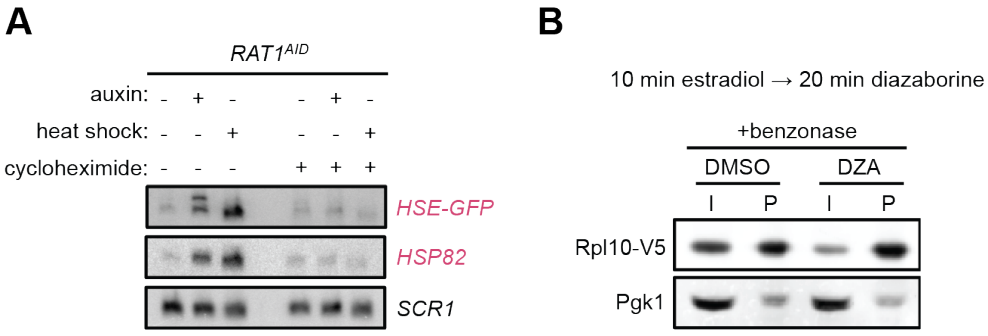

Figure S5. Aggregation of orphan r-proteins during RPAS. (**A**) *RAT1*^{AID} cells were mock or CHX (200 µg/ml, 3 min) treated before addition of auxin or heat shock (37°C) for 20 min. Northern was performed for the Hsf1 reporter transgene *HSE-GFP* consisting of *GFP* downstream of four Hsf1 binding sites (heat shock element, HSE), and *HSP82*. (**B**) Results of treating extracts with benzonase does not prevent the aggregating behavior of newly synthesized Rpl10 when treated with DZA. Experiment was performed as in Figure 4 except extracts contained benzonase to degrade RNA and DNA.

bioRxiv preprint doi: https://doi.org/10.1101/458810; this version posted October 31, 2018. The copyright holder for this preprint (which was not certified by peer review) is the author/funder. All rights reserved. No reuse allowed without permission.

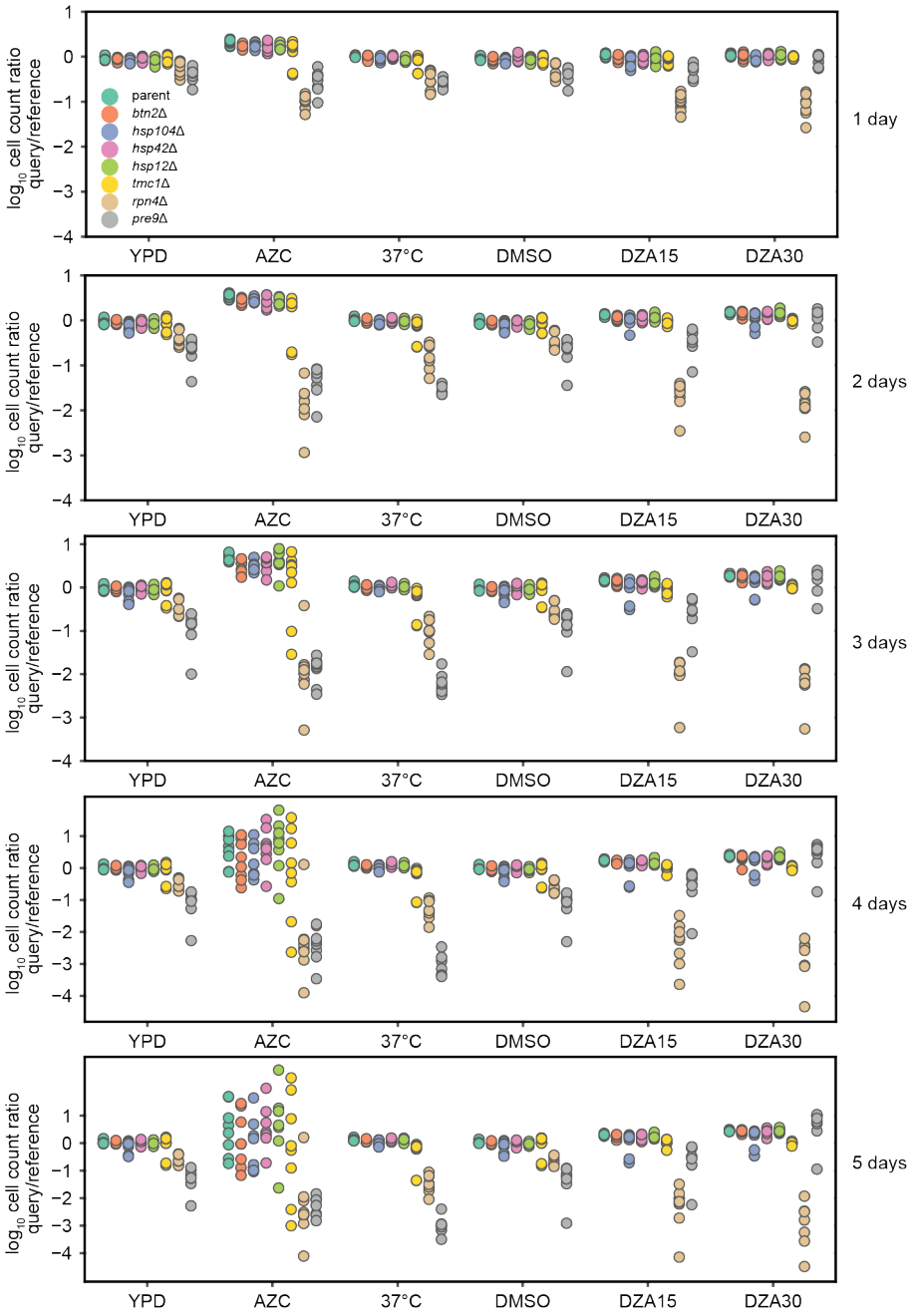

Figure S6. Competitive fitness of strains lacking single Hsf1-dependent genes. Log_{10} ratios of query mCherry to WT reference YFP cells after the indicated number of days of co-culture, normalized to the ratio at t=0. Each dot represents one replicate for a total of 8 replicates per competition. Conditions: YPD, 37ºC, AZC (5 mM), DMSO (vehicle, 0.2%), DZA15 (DZA 15 µg/ml), DZA30 (DZA 30 µg/ml). The query parent (WT), *btn2Δ*, *hsp104Δ*, *hsp42Δ*, and *hsp12Δ* all grew identically under all conditions, suggesting these mutants had no growth defect in any condition. *tmc1Δ* exhibited a mild but reproducible defect in DZA (~4% slower per doubling, $p=2.2 \times 10^{-8}$ by two-sided t-test in "DZA30", no defect in DMSO).

bioRxiv preprint doi: https://doi.org/10.1101/458810; this version posted October 31, 2018. The copyright holder for this preprint (which was not certified by peer review) is the author/funder. All rights reserved. No reuse allowed without permission.

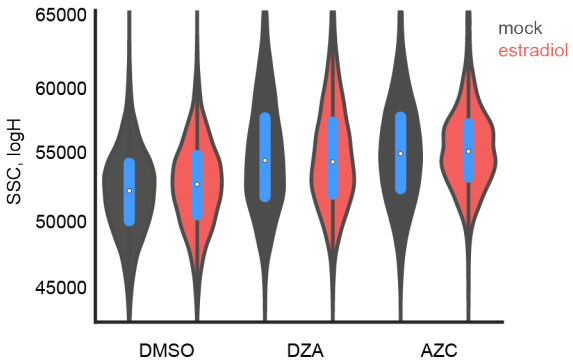

Figure S7. Growth improvement is not due to changes in cell size. The size of distribution of cells from Figure 7A was determined by flow cytometry by side scatter, plotted in log-space for each condition without or with estradiol pre-conditioning.

bioRxiv preprint doi: https://doi.org/10.1101/458810; this version posted October 31, 2018. The copyright holder for this preprint (which was not certified by peer review) is the author/funder. All rights reserved. No reuse allowed without permission.

Supplemental Tables:

Table S1. Yeast strains used in this study.

Name (YBT#)	Description	Background	Genotype	Source	Figures
021	*WT^{AA}*	BY4741	*TOR1-1 fpr1Δ RPL13A-2xFKBP12::NATMX6 RPB3-3xFLAG*	This study	S2F
026	*NRD1^{AA}*	BY4741	*TOR1-1 fpr1Δ RPL13A-2xFKBP12::NATMX6 RPB3-3xFLAG NRD1-FRB-GFP::KANMX6*	This study	S2C, S2F
027	*RAT1^{AA}*	BY4741	*TOR1-1 fpr1Δ RPL13A-2xFKBP12::NATMX6 RPB3-3xFLAG RAT1-FRB-GFP::KANMX6*	This study	S2C, S2F
096	*RAT1^{AA} HSE-GFP*	BY4741	*TOR1-1 fpr1Δ RPL13A-2xFKBP12::NATMX6 RPB3-3xFLAG RAT1-FRB-GFP::KANMX6 ura3Δ0::4xHSE-GFP::URA3*	This study	S2E
100	*RAT1^{AID}*	BY4741	*leu2Δ0::GPD1pr-osTIR1::LEU2 RPB3-3xFLAG RAT1-V5-IAA7::KANMX6*	This study	1C, 1D, 1E, 3A, 3B, S1A, S1B, S1D, S1E, S2A

bioRxiv preprint doi: https://doi.org/10.1101/458810; this version posted October 31, 2018. The copyright holder for this preprint (which was not certified by peer review) is the author/funder. All rights reserved. No reuse allowed without permission.

152	*DXO1^{AID}*	BY4741	*leu2Δ0::GPD1pr-osTIR1::LEU2 DXO1-V5-IAA7::KANMX6*	This study	S2A
154	*RTT103^{AID}*	BY4741	*leu2Δ0::GPD1pr-osTIR1::LEU2 RTT103-V5-IAA7::KANMX6*	This study	S2A
155	*WT^{AID}*	BY4741	*leu2Δ0::GPD1pr-osTIR1::LEU2 RPB3-3xFLAG*	This study	1D, 1E, 3A, 3B, S1D, S1E
156	*RAT1^{AID} HSE-GFP*	BY4741	*leu2Δ0::GPD1pr-osTIR1::LEU2 RPB3-3xFLAG RAT1-V5-IAA7::KANMX6 ura3Δ0::4xHSE-GFP::URA3*	This study	S5A
162	*RAT1^{AA} rqc2Δ*	BY4741	*TOR1-1 fpr1Δ RPL13A-2xFKBP12::NATMX6 RPB3-3xFLAG RAT1-FRB-GFP::KANMX6 rqc2Δ::HIS3MX6*	This study	S1C
171	*RRP17^{AID}*	BY4741	*leu2Δ0::GPD1pr-osTIR1::LEU2 RPB3-3xFLAG RRP17-V5-IAA7::KANMX6*	This study	1C, 1D, 1E, 3A, 3B, S1D
173	*XRN1^{AID}*	BY4741	*leu2Δ0::GPD1pr-osTIR1::LEU2 RPB3-3xFLAG XRN1-V5-IAA7::KANMX6*	This study	S2B

bioRxiv preprint doi: https://doi.org/10.1101/458810; this version posted October 31, 2018. The copyright holder for this preprint (which was not certified by peer review) is the author/funder. All rights reserved. No reuse allowed without permission.

174	*RRP44^{AID}*	BY4741	*leu2Δ0::GPD1pr-osTIR1::LEU2 RPB3-3xFLAG RRP44-V5-IAA7::KANMX6*	This study	1C, 1D, 1E, 3A, 3B, S1D
178	*LAS1^{AID}*	BY4741	*leu2Δ0::GPD1pr-osTIR1::LEU2 RPB3-3xFLAG LAS1-V5-IAA7::KANMX6*	This study	1C, 1D, 1E, 3A, 3B, S1D
187	*HSF1*	W303a	*hsf1Δ::KANMX6 leu2-3,112::HSE-mVenus::LEU2 trp1-1::HSF1pr-HSF1::TRP1*	(Zheng et al., 2016)	6A, 6B
191	*HSF1^{PO4*}*	W303a	*hsf1Δ::KANMX6 leu2-3,112::HSE-mVenus::LEU2 trp1-1::HSF1pr-HSF1^{PO4*}::TRP1*	(Zheng et al., 2016)	6A, 6B
194	Estradiol OE parent	W303a	*ura3-1::GAL4-ER-MSN2^{AD}::URA3*	D. Pincus	
196	*HSF1^{DBD}-VP16*	W303a	*hsf1Δ::KANMX6 his3-11:: GAL4-ER-MSN2^{AD}::HIS3 leu2-3,112::HSE-mVenus::LEU2 trp1-1::GAL1pr-HSF1^{DBD}-VP16::TRP1*	(Zheng et al., 2016)	7A, S7
197	*HSF1* control	W303a	*hsf1Δ::KANMX6 his3-11:: GAL4-ER-MSN2^{AD}::HIS3 leu2-3,112::HSE-mVenus::LEU2 trp1-1::HSF1pr-HSF1::TRP1*	(Zheng et al., 2016)	7B

bioRxiv preprint doi: https://doi.org/10.1101/458810; this version posted October 31, 2018. The copyright holder for this preprint (which was not certified by peer review) is the author/funder. All rights reserved. No reuse allowed without permission.

211	*TSR2^{AID}*	BY4741	*leu2Δ0::GPD1pr-osTIR1::LEU2 RPB3-3xFLAG TSR2-V5-IAA7::KANMX6*	This study	2F
212	*YAR1^{AID}*	BY4741	*leu2Δ0::GPD1pr-osTIR1::LEU2 RPB3-3xFLAG YAR1-V5-IAA7::KANMX6*	This study	2F
215	*GAL-GFP-V5*	W303a	*ura3-1::GAL4-ER-MSN2^{AD}::URA3 his3-11::GAL1pr-GFP-V5::HIS3*	This study	3E, 4D, 4F
216	*GAL-RPS3-V5*	W303a	*ura3-1::GAL4-ER-MSN2^{AD}::URA3 his3-11::GAL1pr-RPS3-V5::HIS3*	This study	3D, 4D, 4F
219	*SQT1^{AID}*	BY4741	*leu2Δ0::GPD1pr-osTIR1::LEU2 RPB3-3xFLAG SQT1-V5-IAA7::KANMX6*	This study	2F
223	*GAL-RPL3-V5*	W303a	*ura3-1::GAL4-ER-MSN2^{AD}::URA3 his3-11::GAL1pr-RPL3-V5::HIS3*	This study	3E, 4D, 4E, 4F
224	*GAL-RPL4-V5*	W303a	*ura3-1::GAL4-ER-MSN2^{AD}::URA3 his3-11::GAL1pr-RPL4-V5::HIS3*	This study	4D, 4F
225	*GAL-RPL10-V5*	W303a	*ura3-1::GAL4-ER-MSN2^{AD}::URA3 his3-11::GAL1pr-RPL10-V5::HIS3*	This study	3E, 4D, 4E, 4F, S5B

bioRxiv preprint doi: https://doi.org/10.1101/458810; this version posted October 31, 2018. The copyright holder for this preprint (which was not certified by peer review) is the author/funder. All rights reserved. No reuse allowed without permission.

226	*GAL-RPS26-V5*	W303a	*ura3-1::GAL4-ER-MSN2^{AD}::URA3 his3-11::GAL1pr-RPS26-V5::HIS3*	This study	4D, 4F
232	mCherry query parent	FY4	*HO::mCherry::KANMX6*	This study	6D, S5
235	*rpn4Δ* query	FY4	*HO::mCherry::KANMX6 rpn4Δ::NATMX6*	This study	6D, S5
236	*tmc1Δ* query	FY4	*HO::mCherry::KANMX6 tmc1Δ::NATMX6*	This study	S5
237	*hsp104Δ* query	FY4	*HO::mCherry::KANMX6 hsp104Δ::NATMX6*	This study	S5
238	*hsp26Δ* query	FY4	*HO::mCherry::KANMX6 hsp26Δ::NATMX6*	This study	S5
239	*pre9Δ* query	FY4	*HO::mCherry::KANMX6 pre9Δ::NATMX6*	This study	S5
240	*btn2Δ* query	FY4	*HO::mCherry::KANMX6 btn2Δ::NATMX6*	This study	S5
241	*hsp42Δ* query	FY4	*HO::mCherry::KANMX6 hsp42Δ::NATMX6*	This study	S5
242	*hsp12Δ* query	FY4	*HO::mCherry::KANMX6 hsp12Δ::NATMX6*	This study	S5
243	TB50a	TB50a		T. Powers	1G (rap)

bioRxiv preprint doi: https://doi.org/10.1101/458810; this version posted October 31, 2018. The copyright holder for this preprint (which was not certified by peer review) is the author/funder. All rights reserved. No reuse allowed without permission.

256	*HSE-Venus*	BY4741	*leu2Δ::HSE-mVenus:LEU2*	This study	4A
259	*DRG1*	BY4741	*drg1Δ::NATMX6* pBT124 (pRS316 *DRG1 URA3* CEN/ARS)	This study	S3
260	*DRG1^{V725E}*	BY4741	*drg1Δ::NATMX6* pBT125 (pRS316 *DRG1^{V725E} URA3* CEN/ARS)	This study	S3
261	YFP reference	FY4	*HO::YFP::KANMX6*	This study	6D
	Sis1-YFP/Cfi1-mKate	W303a	*SIS1-YFP CFI1-mKate*	D. Pincus	5A, 5B, 5C
	Hsp104-mKate	W303a	*leu2-3,112::HSP104-mKate::LEU2*	D. Pincus	5D
	W303a parent	W303a	*ADE2*	D. Pincus	
		BY4741	*RPB3-3xFLAG::NATMX6*	(Churchman and Weissman, 2011)	1E, 2D, 3A, 3B (diamide RNA-seq)
	Anchor-away parent	BY4741	*TOR1-1 fpr1Δ RPL13A-2xFKBP12::NATMX6*	F. Holstege	
		BY4741		Euroscarf	1E (diamide), 1G (CHX), 2B, 2C, 2D, 3A, 3B, 3F, 4C, S4

bioRxiv preprint doi: https://doi.org/10.1101/458810; this version posted October 31, 2018. The copyright holder for this preprint (which was not certified by peer review) is the author/funder. All rights reserved. No reuse allowed without permission.

Parental genotypes:

FY4:	*MATa*
BY4741:	*MATa his3Δ1 leu2Δ0 met15Δ0 ura3Δ0*
W303a:	*MATa leu2-3,112 trp1-1 can1-100 ura3-1 his3-11,15 ADE2+*
TB50a:	*MATa leu2-3,112 ura3-52 rme1 trp1 his4*

bioRxiv preprint doi: https://doi.org/10.1101/458810; this version posted October 31, 2018. The copyright holder for this preprint (which was not certified by peer review) is the author/funder. All rights reserved. No reuse allowed without permission.

Table S2. Plasmids used in this study.

Name	Plasmid	Use	Reference/source
	pFA6a *FRB-GFP::KANMX6*	C-terminal tagging for anchor-away	(Haruki et al., 2008)
L260	pFA6a *V5-IAA7::KANMX6*	C-terminal tagging for AID	F. Winston
pTIR4	pNH605 *GPD1pr-OsTIR1::LEU2*	Integrate *OsTIR1* at *LEU2*	F. Winston
pZM467	*3xFLAG-URA3-3xFLAG*	Scarless C-terminal FLAG-tagging	(Moqtaderi and Struhl, 2008)
pVD302	*4xHSE-GFP::URA3*	Insert *HSE-GFP* reporter at *URA3*	*(Solís et al., 2016)*
pDP122	pNH605 *4xHSE-mVenus::LEU2*	Insert *HSE-mVenus* reporter at *LEU2*	(Zheng et al., 2016)
	pFA6a *HIS3MX6*	Gene deletion with *HIS3*	Euroscarf
	pFA6a *NATMX6*	Gene deletion with *NAT*	Euroscarf
	pNH603 *GAL1pr::HIS3*	Integrate V5-tagged ORFs for induction by estradiol (GEM)	D. Pincus
pBT124	pRS316 *DRG1 URA3 CEN/ARS*	*DRG1* plasmid cover	This study
pBT125	pRS316 *DRG1*^{V725E} *URA3 CEN/ARS*	*DRG1*^{V725E} plasmid cover	This study

bioRxiv preprint doi: https://doi.org/10.1101/458810; this version posted October 31, 2018. The copyright holder for this preprint (which was not certified by peer review) is the author/funder. All rights reserved. No reuse allowed without permission.

Table S3. Primers used in this study for ChIP-qPCR and Northern blotting. Primers for cloning and strain construction were designed using standard techniques and are available upon request.

Name	Target	Use	Sequence
oBT220	*GFP* RNA	Northern (PCR/dsDNA)	CCAAAGGAGAAGAACTTTTC
oBT221	*GFP* RNA	Northern (PCR/dsDNA)	ATGCCGTTTCATATGATCTG
oBT271	*SCR1* RNA	Northern (Oligo)	GTCTAGCCGCGAGGAAGG
oBT305	*HSP82* RNA	Northern (PCR/dsDNA)	CATGCAGATGCCCTATTTAC
oBT306	*HSP82* RNA	Northern (PCR/dsDNA)	GAACATCATGGCCTTGAATA
oBT313	*TPS2* RNA	Northern (PCR/dsDNA)	GACATGTTGAAGGGAATCAG
oBT314	*TPS2* RNA	Northern (PCR/dsDNA)	CTAAAGTCTCCAGGACTTGC
oBT319	*BTN2* RNA	Northern (PCR/dsDNA)	GCGAAAGAACCACTAACCAA
oBT320	*BTN2* RNA	Northern (PCR/dsDNA)	AGAGATAGGCAATGATTTGG
oBT361	5.8*S* pre-rRNA (017)	Northern (Oligo)	GCGTTGTTCATCGATGC
oBT509	35*S* pre-rRNA (800)	Northern (Oligo)	GCAAAGATATGAAAACTCCAC
oBT524	*mVenus* RNA	Northern (PCR/dsDNA)	GGTTATGGTTTGCAATGTTTTG
oBT525	*mVenus* RNA	Northern (PCR/dsDNA)	CCATTCTTTTGTTTGTCAGC
oBT526	*GAL7* RNA	Northern (PCR/dsDNA)	CCTTGGTTAGGTCAACAGGAG
oBT527	*GAL7* RNA	Northern (PCR/dsDNA)	AGTCGCATTCAAAGGAGCC
oBT528	*GAL10/lncGAL 10* RNA	Northern (PCR/dsDNA)	GCATCACATTCCCTTCTATGAG
oBT529	*GAL10/lncGAL 10* RNA	Northern (PCR/dsDNA)	ACGATTAGCATACCTGCCG
SD189	*HSP12* RNA	Northern (PCR/dsDNA)	TCTGACGCAGGTAGAAAAGG

bioRxiv preprint doi: https://doi.org/10.1101/458810; this version posted October 31, 2018. The copyright holder for this preprint (which was not certified by peer review) is the author/funder. All rights reserved. No reuse allowed without permission.

SD190	*HSP12* RNA	Northern (PCR/dsDNA)	GTTGGGTCTTCTTCACCG
oBT335	*HSP82* promoter	ChIP-qPCR	GTCACATATTGTTCGAACAATTCTGG
oBT336	*HSP82* promoter	ChIP-qPCR	CTTCCACGGCGTTCTAGAAAAAAAAG
oBT337	*HSP104* promoter	ChIP-qPCR	CTTAAACGTTCCATAAGGGGC
oBT338	*HSP104* promoter	ChIP-qPCR	TGCAGTTCTTTGAGATGGGCC
oBT339	*SSA4* promoter	ChIP-qPCR	GCCGCACATCCATTCCGGTATG
oBT340	*SSA4* promoter	ChIP-qPCR	CGGGCAAAAGATATCCGCTTTG
oBT341	*ARS504* promoter	ChIP-qPCR	GTCAGACCTGTTCCTTTAAGAGG
oBT342	*ARS504* promoter	ChIP-qPCR	CATACCCTCGGGTCAAACAC

bioRxiv preprint doi: https://doi.org/10.1101/458810; this version posted October 31, 2018. The copyright holder for this preprint (which was not certified by peer review) is the author/funder. All rights reserved. No reuse allowed without permission.

Table S4 (separate Excel file). Gene annotation lists and RNA-seq data. Tab “Gene_Lists” contains members of groups used for analysis. Subsequent tabs contain RNA abundance measurements determined by DESeq2 or RPKM calculations.

Table S5 (separate Excel file). Flow cytometry data from competitive fitness experiments. Query (mCherry) and reference (YFP) counts for each competition at t=0, 1, 2, 3, 4, 5 days. Each mutant query had four isolates (“Iso1-4”) that were tested in two technical replicates (“Rep1-2”, for a total of eight replicates per experiment. The normalized, $\log_{10}$ transformed values were used to generate plots.